ACS OMEGA

Open Access

http://pubs.acs.org/journal/acsodf

Review

Unleashing Vanadium-Based Compounds for High-Energy Aqueous Zinc−Ion Batteries

Saad Zafar and Bimlesh Lochab*

Cite This: *ACS Omega* 2024, 9, 47920−47938

Read Online

ACCESS | Metrics & More | Article Recommendations

ABSTRACT: Rechargeable aqueous zinc−ion batteries (ZIBs) are poised as a promising solution for large-scale energy storage and portable electronic applications. Their appeal lies in their affordability, abundant materials, high safety standards, acceptable energy density, and eco-friendliness. Vanadium-based compounds stand out as potential cathode materials due to their versatile phases and variable crystal structures, empowering design flexibility to affect the theoretical capacity. However, challenges, such as V dissolution and substantial capacity degradation, have hindered their widespread use. Recent breakthroughs in crafting innovative V-based materials for aqueous ZIBs, by preintercalating guest species, have significantly bolstered structural stability and facilitated faster charge migration, leading to enhanced capacity and stable cycling. This review delves into the latest advancements in vanadium-based cathodes with preintercalated guest species, examining their altered crystal structures and the mechanisms involved in Zn^{2+} ion storage. It also investigates how different guest materials within these cathodes impact the electrochemical capacity. Additionally, this assessment identifies key obstacles impeding progress and proposes potential solutions while also anticipating the future trajectory of aqueous ZIBs. These insights are invaluable to researchers and manufacturers alike, offering a roadmap for commercialization.

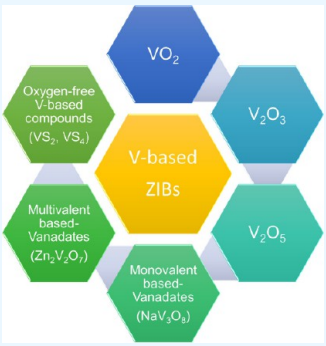

1. INTRODUCTION

Globally, the development of electrochemical energy storage and conversion technologies that are safe, cost-effective, sustainable, and efficient has increased to mitigate rising concerns about climate change and environmental pollution. Lithium−ion batteries (LIBs) offer high energy density, have been extensively used in portable devices, and are being considered for electric cars. However, limited lithium reserves, price fluctuations, and safety are major concerns. Alternative battery chemistries that utilize elements such as sodium (Na), potassium (K), magnesium (Mg), aluminum (Al), and zinc (Zn) have garnered significant interest.[1−3] Rechargeable zinc−ion batteries (ZIBs) exhibit significant potential due to their superior ambient stability and a lower cost of Zn (∼US \$2.4 kg^{-1}) compared to alkali metals (e.g., Li ∼US \$19.2 kg^{-1}; Na ∼US \$3.1 kg^{-1}; K ∼US \$13.1 kg^{-1}).[3−5] There is a wide availability of lower cost cathode materials like MnO_2 (∼US \$1.7 kg^{-1}) and V_2O_5 (∼US \$5.5 kg^{-1}) for ZIBs compared to LIBs (e.g., $LiCoO_2$, ∼US \$55 kg^{-1} and $Li(NiMnCo)O_2$, ∼US \$34 kg^{-1}).[2,3,6] Additionally, the commonly employed aqueous electrolyte for ZIBs is cost-effective, possesses excellent safety, and exhibits high ionic conductivity (0.1−6 S cm^{-1}) in comparison to that of the combustible organic electrolytes used in LIBs (10^{-3}−10^{-2} S cm^{-1}). ZIBs based on a Zn anode, a vanadium oxide cathode, and an aqueous $ZnSO_4$ electrolyte have a lower estimated cost (\$65 per kWh vs ∼\$300 per kWh, LIB).[2] ZIBs have significant prospects for practical applications compared to other metal ion batteries (Figure 1a).

A diverse battery technology such as Zn−MnO_2, Zn−NiOOH, Zn−Ag_2O, and Zn−air batteries has evolved since their invention in the year 1799. Initially developed alkaline KOH-electrolyte based Zn−MnO_2 batteries faced the prime issues of the uncontrolled growth of zinc dendrites and the formation of insulating, irreversible ZnO byproducts.[8,9] Alternately, moderately acidic aqueous electrolytes in ZIBs are explored.[10] Figure 1b illustrates the components of a typical rechargeable ZIB, including a metallic Zn anode, a Zn^{2+} storage cathode, and a Zn^{2+}−salt electrolyte. Rechargeable ZIBs function by reversibly (de)intercalating Zn^{2+} at the cathode and plating and stripping Zn at the anode during the process of discharging/charging.

Aqueous zinc−ion batteries (ZIBs), which utilize a zinc metal anode and water-based electrolytes, are emerging as promising alternatives to traditional LIBs due to several advantageous features: 1) ZIBs leverage the inherent benefits of aqueous electrolytes, such as high ionic conductivity, intrinsic nonflammability, and environmental friendliness. 2) Zinc, as an anode material, offers a low electrochemical

Received: July 9, 2024
Revised: October 17, 2024
Accepted: November 5, 2024
Published: November 26, 2024

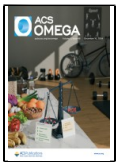

https://doi.org/10.1021/acsomega.4c06199
ACS Omega 2024, 9, 47920−47938

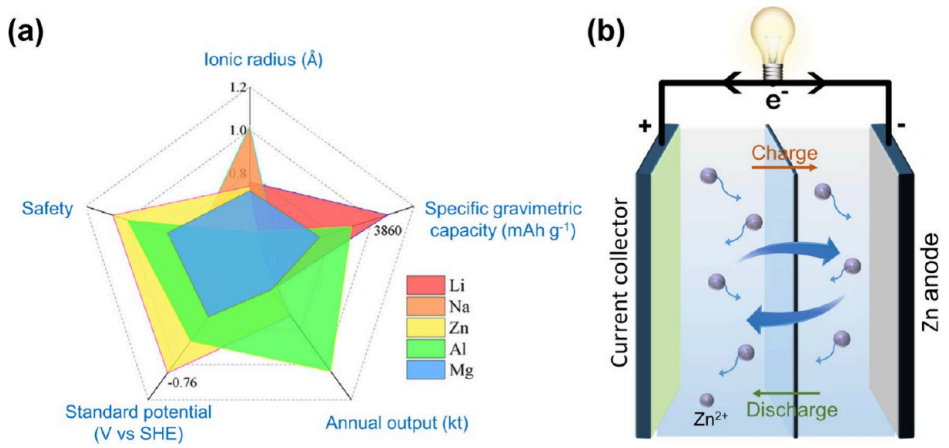

Figure 1. (a) Comparison of various metal−ion batteries using a "Radar Diagram". Reproduced with permission from ref 7. Copyright 2021, Elsevier. (b) Schematic illustration of the working principle of rechargeable zinc−ion batteries.

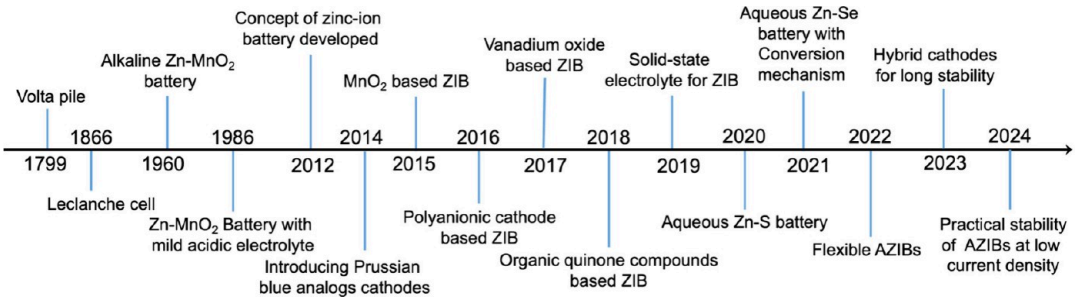

Figure 2. Brief development history of rechargeable zinc−ion batteries.

reduction potential of −0.76 V vs SHE and high theoretical capacities of 820 mAh g^{-1} and 5855 mAh cm^{-3} for gravimetric and volumetric capacities, respectively. 3) ZIBs present economic benefits compared to other battery systems (such as those based on Li, Na, Mg, and K) because they do not require additional inert atmosphere conditions during manufacturing, due to the natural compatibility of zinc with water and the low cost of electrode materials.

A wide variety of materials are explored, such as cathodes, anodes, and electrolytes, and their inter-relationships are reported. Representative cathodic materials that have been extensively investigated are listed in Figure 2. These include manganese-based, vanadium-based, Prussian blue analogues, conducting polymer (CP) composites, organic materials, and others. Nevertheless, cathodes based on vanadium (V) are regarded as highly promising owing to the unique and inherited physical and chemical features exhibited by V. The multiple oxidation state of V allows a wide range of charge−discharge voltages leading to high energy density with significant pseudocapacitance and steady storage capabilities. These characteristics empower extended life cycle, appreciable charge capacity, and power density. Further, vanadium compounds often show distinct chemical compositions and structural morphologies affecting electrochemical behavior.[11] The open structures facilitate ion insertion and extraction.[12] Despite attractive properties, dissolution of V-based materials within electrolytes requires attention. However, this issue is relatively less pronounced compared to other cathode contenders such as organics and manganese oxides.[13,14] The wide gallery spacing and morphologies offered by V-based materials allow swift and efficient (de)insertion of zinc ions consequently, expanding their utility for zinc storage batteries.

Presently, the primary focus of research on cathodes based on vanadium is explored as vanadium oxides, vanadates, and oxygen-free V-based compounds such as VS_2.[7] Vanadates formed via cationic preintercalation of vanadium oxides exhibit enhanced zinc−ion storage capacity.[15] The guest cations within the vanadium interlayer are securely attached through robust ionic bonds connecting the two neighboring layers, forming a robust expanded layered stable architecture, advantageous for structural reversibility. The nature, type, and number of intercalants within vanadium-based cathodes have a substantial impact on the electrochemical performance.[16] A significant advancement has been made in the recent past on exploration of these chemistries, and thus it is imperative to review a comprehensive examination of the vanadate cathodes, pertaining to the mechanism and cathode design. Our focus will be on the design strategies employed for the cathode, crystal structure, electrochemical performance, and reaction mechanism.

2. ENERGY STORAGE MECHANISM IN ZIBS

Unlike the well-established lithium/sodium-ion-based energy storage chemistries based on insertion, conversion, and alloying reactions for storing monovalent alkali metal cations, the proposed reaction mechanism in aqueous ZIB systems is complex and subject to debate. The redox processes in aqueous ZIB systems primarily occur through three mechanisms: Zn^{2+} insertion/extraction,[2,17,18] chemical conversion reaction,[4] and H^+/Zn^{2+} insertion/extraction.[19,20] A summary of the mechanisms reported is explained in the section below.

https://doi.org/10.1021/acsomega.4c06199
ACS Omega 2024, 9, 47920−47938

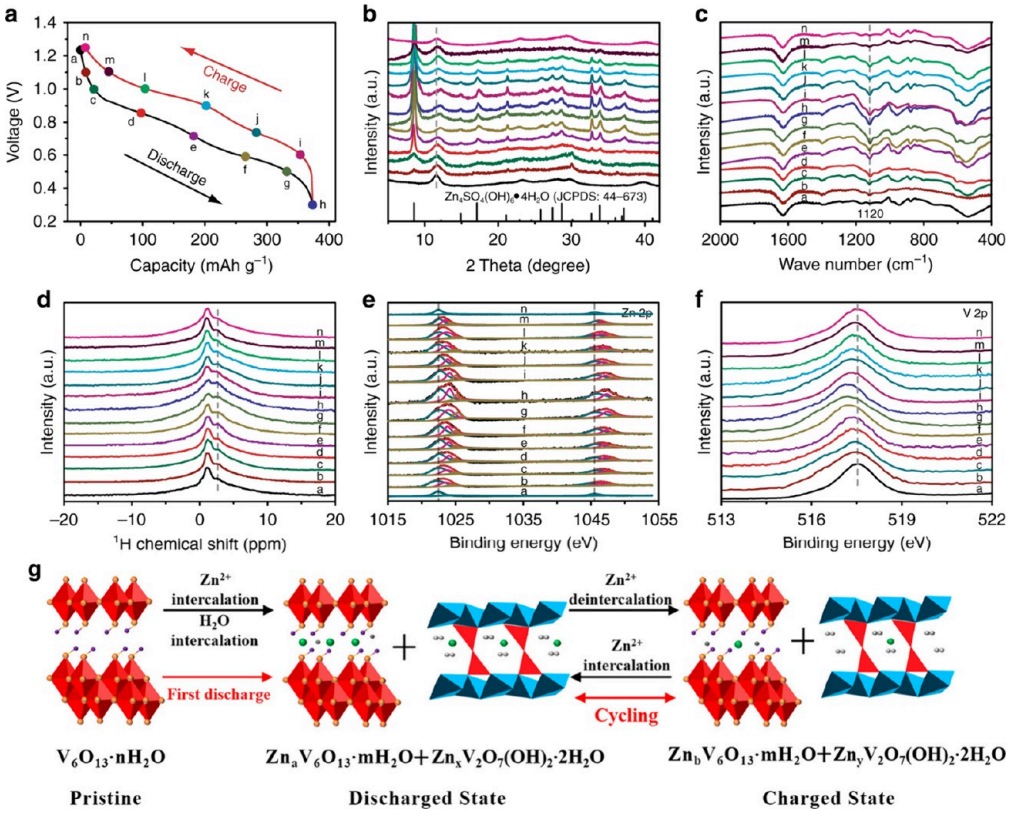

Figure 3. Simultaneous H^+ and Zn^{2+} insertion/extraction mechanism. (a) Second charge/discharge curve of NVO nanobelts at 0.1 A g^{-1}. Ex situ (b) XRD patterns, (c) FTIR spectra, (d) solid state ^1H NMR, and XPS spectra of (e) Zn 2p and (f) V 2p at selected states. (g) Schematic diagram of the conversion reaction mechanism for $V_6O_{13}{\cdot}nH_2O$. (a–f) Reproduced with permission from ref 31. Copyright 2018, Nature. (g) Reproduced with permission from ref 32. Copyright 2019, American Chemical Society.

2.1. Zn^{2+} Insertion/Extraction Mechanism. Compounds with tunnel- and layered-type structures facilitate the process of introducing or removing Zn^{2+} (ionic radii 0.74 Å < interlayer spacing) from their respective hosts, while the charge storage mechanism occurred via a typical Zn^{2+} insertion/extraction reaction mechanism between tunnels of the two electrodes, as presented below (M stands for cathode material):

Cathode:

$$xZn^{2+} + 2xe^- + M \leftrightarrow Zn_xM$$

Anode:

$$Zn \leftrightarrow Zn^{2+} + 2e^-$$

Nazar et al.[2] advanced the field with the use of Zn/vanadium-based oxides batteries with cathode inherently possessing zinc ions, $Zn_{0.25}V_2O_5{\cdot}nH_2O$. Intercalation of water upon immersion in the electrolyte modified the structure of pristine $Zn_{0.25}V_2O_5{\cdot}nH_2O$, expanding the galleries for easy Zn^{2+} intercalation, with a notable highly reversible insertion/extraction of 1.1 Zn^{2+} ions during the discharge/charge reaction, as indicated by the following equation:

$$Zn_{0.25}V_2O_5{\cdot}nH_2O + 1.1Zn^{2+} + 2.2e^- \leftrightarrow Zn_{1.35}V_2O_5{\cdot}nH_2O$$

Prussian blue analogues (PBAs)[21−26] and polyanionic olivine-based phosphates $MNPO_4$ (M = Li, Na, K; N = V, Fe, Mn, Ni, Co, etc.)[27−30] facilitate the insertion/extraction of Zn^{2+} ions due to their open framework. The processes at the cathode electrode in these compounds entail the movement of Zn^{2+} ions into and out of their 3D network, whereas the reactions at the anode electrode are associated with the deposition and dissolution of zinc.

2.2. H^+ and Zn^{2+} Insertion/Extraction Mechanism. Host materials that possess open channels or a layered architecture have the potential to facilitate the simultaneous entry of H^+ and Zn^{2+} ions. Vanadium-based oxides ($NaV_3O_8{\cdot}1.5H_2O$, NVO) reported by Wan et al.[31] have a cointercalation mechanism of Zn^{2+} and H^+ (Figure 3a). The $Zn_4SO_4(OH)_6{\cdot}4H_2O$ phase (JCPDS: 39-688) was observed through ex situ XRD characterization (Figure 3b). This phase was formed by the reaction of OH^- with $ZnSO_4$ and H_2O, suggesting that additional H^+ would be incorporated into the NVO host to maintain neutrality of the battery system. The formation of $Zn_4SO_4(OH)_6{\cdot}4H_2O$ was further verified by Fourier transform infrared spectroscopy (FTIR) (Figure 3c). The peak intensity of $Zn_4SO_4(OH)_6{\cdot}4H_2O$ at 1120 cm^{-1} exhibited a progressive increase during discharge. The continuous insertion of H^+ into NVO during discharge was verified using ex situ solid-state nuclear magnetic resonance (Figure 3d). By using the X-ray photoelectron spectroscopy (XPS) characterization technique, it was also possible to witness the insertion of Zn^{2+} into $Zn_4SO_4(OH)_6{\cdot}4H_2O$. This indicates that Zn^{2+} took part in the energy storage of the $Zn/NaV_3O_8{\cdot}1.5H_2O$ system (Figure 3e,f). Consequently, the $Zn//NaV_3O_8{\cdot}1.5H_2O$ battery energy storage mechanism differs from the conventional energy storage mechanism (which only uses zinc−ion intercalation/deintercalcation), but it shares the same process of H^+ and Zn^{2+} intercalation/deintercalation, which is the primary cause of its superior electrochemical performance. In this way, the

https://doi.org/10.1021/acsomega.4c06199
ACS Omega 2024, 9, 47920−47938

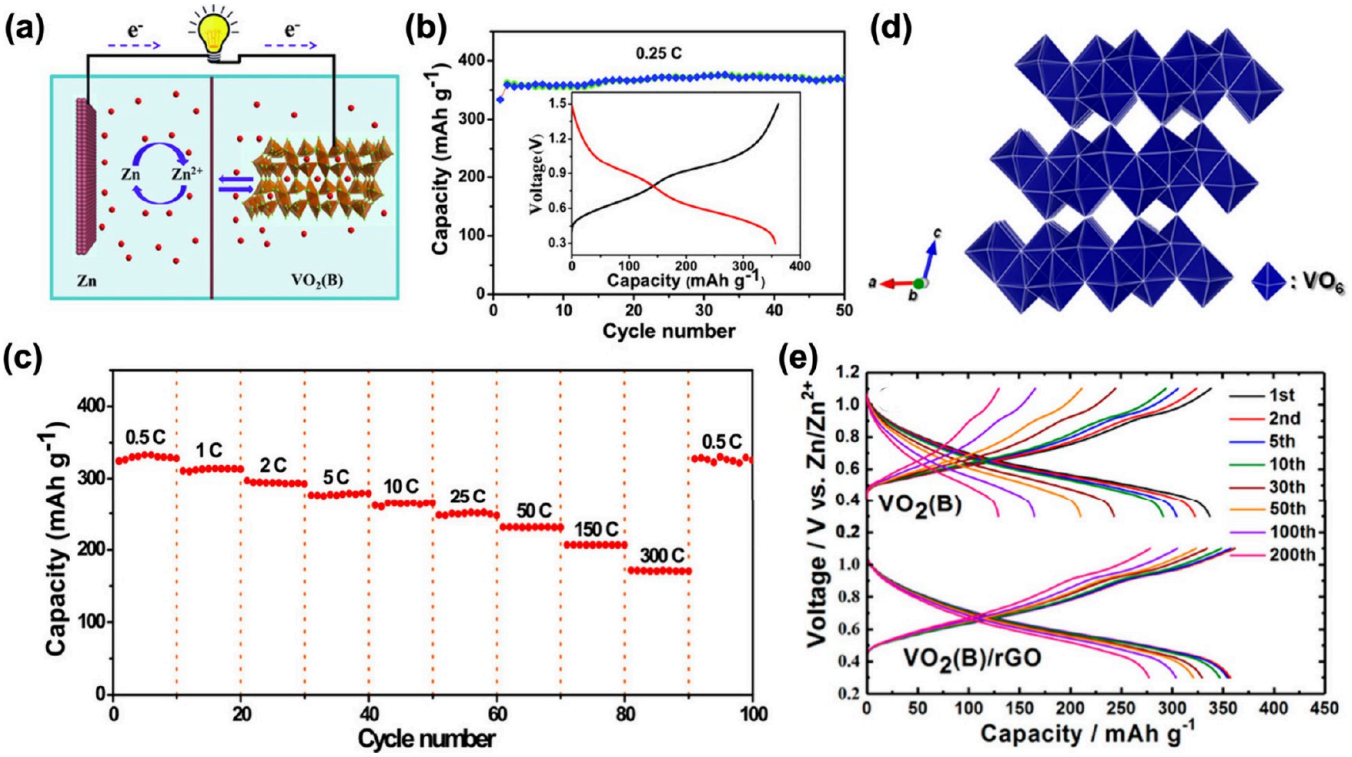

Figure 4. VO_2(B) nanofiber cathode: (a) Schematic of AZIB with Zn foil as anode, (b) cycling performance at 0.25 C (additional: GCD curve), and (c) rate capabilities. Reproduced with permission from ref 49. Copyright 2018, Wiley-VCH. (d) Crystal structure. (e) Continuous cycles of the electrode as bare and composite. Reproduced with permission from ref 46 Copyright 2018, American Chemical Society.

insertion and extraction of both Zn^{2+} and H^+ occurred simultaneously in the same step and demonstrated a high capacity of 380 mAh g^{-1}. During the charge and discharge process, stability to the V_3O_8 layers is provided by both sodium ions and water, which functioned as the support structures.

2.3. Chemical Conversion Reaction Mechanism. In addition to the reversible Zn^{2+} insertion/extraction and H^+/Zn^{2+} coinsertion/extraction mechanisms, Liu's group proposed a third reaction mechanism involving the conversion process between α-MnO_2 and MnOOH.[33] Several vanadium-based cathode materials, including atomic layer deposition-derived V_2O_5 (ALD-V_2O_5),[34] V_2O_3@C,[35] and $V_6O_{13}{\cdot}nH_2O$[32] (Figure 3g), have been demonstrated to operate based on this conversion reaction mechanism for zinc-ion energy storage. For instance, $V_6O_{13}{\cdot}nH_2O$ initially reacts with Zn^{2+} ions and water to form $Zn_aV_6O_{13}{\cdot}mH_2O$ and $Zn_xV_2O_7(OH)_2{\cdot}2H_2O$. Subsequently, after the first cycle, the phases evolve into $Zn_bV_6O_{13}{\cdot}mH_2O$ and $Zn_yV_2O_7(OH)_2{\cdot}2H_2O$ (where $a > b$; $x > y$), maintaining a reversible reaction during subsequent cycles. The corresponding electrochemical mechanism of $Zn/V_6O_{13}{\cdot}nH_2O$ can be displayed as follows.

Anode:

$$Zn \leftrightarrow Zn^{2+} + 2e^-$$

Cathode:

$$V_6O_{13}{\cdot}nH_2O + (a + x)Zn^{2+} + 2(a + x)e^- + (m - n + 2)H_2O \leftrightarrow$$

$$Zn_aV_6O_{13}{\cdot}mH_2O + Zn_xV_2O_7(OH)_2{\cdot}2H_2O$$

(In the initial discharge process)

$$Zn_aV_6O_{13}{\cdot}mH_2O + Zn_xV_2O_7(OH)_2{\cdot}2H_2O \leftrightarrow Zn_bV_6O_{13}{\cdot}mH_2O + Zn_yV_2O_7(OH)_2{\cdot}2H_2O + (a + x - b - y)Zn^{2+} + (a + x - b - y)e^-$$

(In the subsequent cycles)

In contrast to the Zn^{2+} insertion/extraction and H^+/Zn^{2+} coinsertion/extraction mechanisms, the conversion reaction mechanism is significantly influenced by the host materials due to the strong electrostatic interactions between Zn^{2+} ions and the host. This mechanism often involves phase transitions or alterations in the crystal structure at different stages of the discharge process. Structural defects introduced during these transitions can impact the electrochemical transfer kinetics of the materials by exposing additional active sites, thereby facilitating the release and storage of Zn^{2+} ions in the cathodes.

3. VANADIUM-BASED CATHODIC MATERIALS FOR HIGH PERFORMANCE AND LONG-LIFE CYCLE

Vanadium is an attractive source for cathodic materials in batteries due to its natural abundance, low cost, and nontoxic nature. The notable characteristics such as extended array oxidation states, enhanced metallic ion hosting capacity, adjustable interlayer spacing, and diverse crystalline composition are additional features enabling their suitability as in lithium−ion batteries (LIBs), nickel−ion batteries (NIBs), and

https://doi.org/10.1021/acsomega.4c06199
ACS Omega 2024, 9, 47920−47938

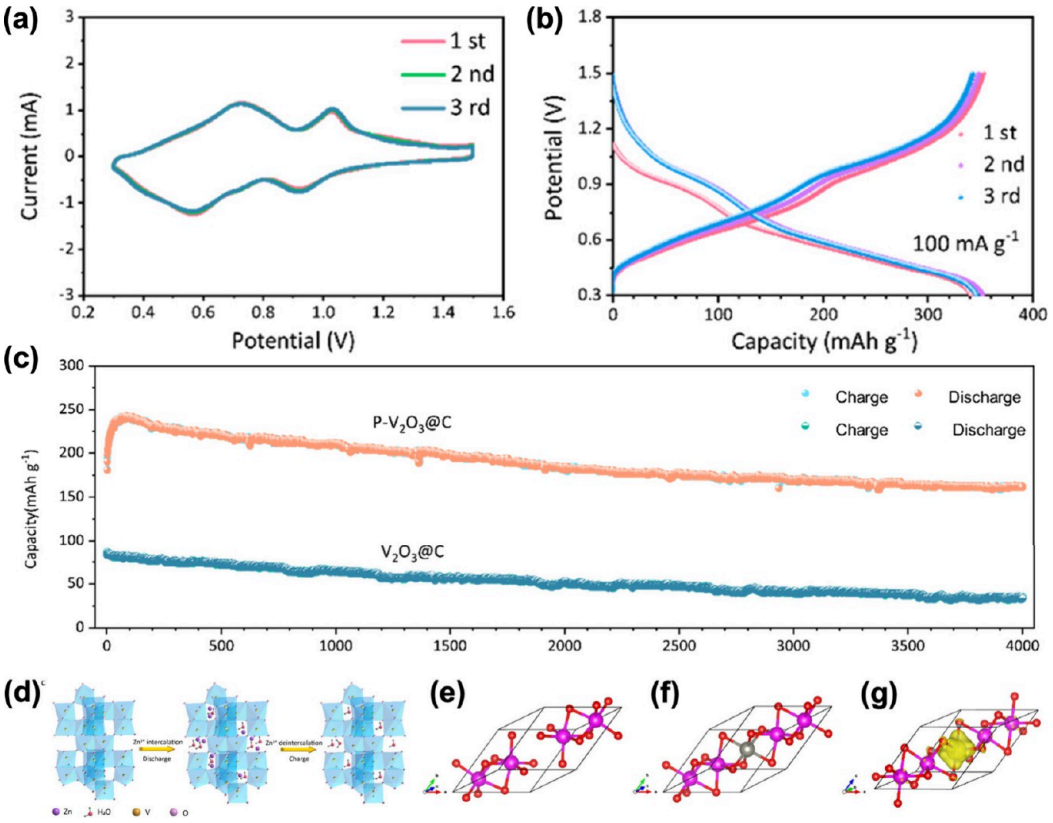

Figure 5. (a) CV at 0.2 mV/s between 0.3 and 1.5 V and (b) charge/discharge curves (GCD) for the initial three cycles of the porous V_2O_3@C microsphere (P-V_2O_3@C). (c) Long-term cycling performance at 5 A g^{-1}. (d) Schematic diagram of the Zn^{2+} storage mechanism. The structure of V_2O_3 without (e) and with (f) Zn^{2+} being inserted. (g) Differential charge state density between V_2O_3 and the inserted Zn ions. Reproduced with permission from ref 57. Copyright 2019, American Chemical Society.

AZIBs.[36,37] Most of the vanadium structures exhibit stability for the existing few components, especially alkaline metals, due to the formation of strong covalent bonds within the substance.[38] Despite their comparatively low voltage level, vanadium-based cathodes are favored due to their multivalency, leading to an increased capacity and extended life cycles. Numerous valence states of vanadium (+5, + 4, + 3, and even +2) account for multielectron redox processes with fast kinetics, and the availability of a diverse array of adaptable morphological structures has a substantial impact on their advancement as noble materials for AZIBs.[39,40] Furthermore, the phenomenon of pseudocapacitance has expedited the use of V cathodes within the realm of energy storage. The pseudocapacitance not only enables rapid and reversible reactions on the cathodic surface but also effectively balances both swift energy transfer and storage capacity, resulting in a battery system that can perform at an ultrahigh rate. Despite significant advancements in vanadium-based cathodic materials, the issue of dissolution and weak bonding among crystal layers led to capacity deterioration. Recently, significant efforts have been made in designing and synthesizing vanadium-based cathodic materials as vanadium oxides, vanadates, and oxygen-free vanadium sourced compounds and their exploration with innovative fabrication yet facile methodologies.[41−43]

3.1. Vanadium Oxides. Vanadium oxides offer a unique combination of structural flexibility and remarkable stability, which distinguishes them from their counterparts. Multiple oxidation states in vanadium allow various compositional structural tunabilities and standard octahedron (standard and deformed), tetrahedron, trigonal bipyramid, and square pyramid, via V−O coordination.[40] The transformation of vanadium polyhedrons leads to the formation of a diverse range of V-oxides with varying structures. This section pertains to the functionality, performance, and efficiency of an alternative variant of V-oxides as a cathodic material, demonstrating their ability to fabricate high performance AZIBs with prolonged stability.

(*i*) VO_2. In this metal oxide, phase transition occurs at a mild temperature, altering the structure which shows a reversible transformation of infrared light from transmission to reflection.[44] The VO_2 phase with different space groups (B ($C2/m$), M ($P2_1/c$), A ($P4_2/nmc$), and D ($P2/c$)) has been widely studied as the cathode material for AZIBs. Furthermore, VO_2 possesses a d^1 electronic state and exhibits several crystal forms with the same chemical formula, such as thermodynamically stable rutile VO_2(R), monoclinic VO_2(M), metastable tetragonal VO_2(A), and monoclinic VO_2(B), VO_2(C), and VO_2(D).[45] Varied crystal structures and electronic configurations account for distinct properties.[46−48] Interestingly, the open structure of metastable monoclinic VO_2(B) possesses the tunnel structure necessary for Zn^{2+} migration, offering a high theoretical capacity, thus making it a viable material for exploration as an electrode in AZIBs. Ding et al.[49] studied the interaction behavior of Zn^{2+} with VO_2(B) in AZIBs assembled with VO_2(B) nanofibers as the cathode, Zn foil as the anode, and $Zn(CF_3SO_3)_2$ as the electrolyte (Figure 4a). VO_2(B) exhibited a high specific capacity of 357 mAh g^{-1} (Figure 4b) and rate capability of 171 mAh g^{-1} at 51.2 A g^{-1}, as shown in Figure 4c. These findings can be attributed to the intercalation pseudocapacitance behavior and the rapid kinetics of Zn^{2+}

https://doi.org/10.1021/acsomega.4c06199
ACS Omega 2024, 9, 47920−47938

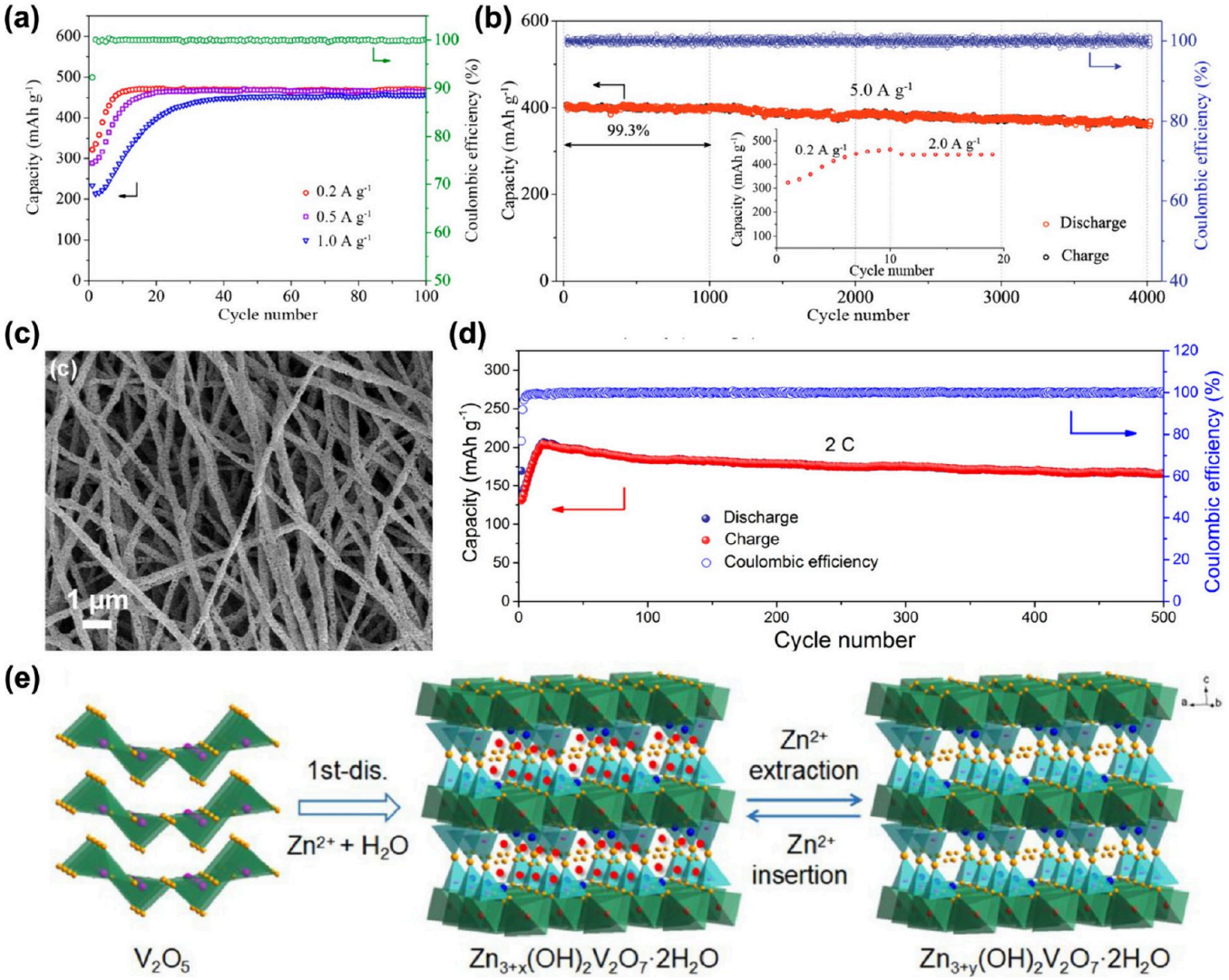

Figure 6. (a) Galvanostatic cycling performance at 0.2, 0.5, and 1.0 A/g and the corresponding Coulombic efficiency at 0.2 A/g. (b) Long-cycling performance at 5.0 A/g (additional capacity evolution in the initial 19 cycles). Reproduced with permission from ref 73. Copyright 2018, American Chemical Society. (c) Scanning electron microscope (SEM) image of porous V_2O_5 nanofibers. (d) Long-term cycle performance of the V_2O_5 cathode at 2 C. (e) Schematic of the reaction mechanism of the V_2O_5 cathode. Reproduced with permission from ref 69. Copyright 2019, Elsevier.

within the tunnel structures of VO_2(B) as supported by *in situ* XRD and electrochemical measurements. Park et al.[46] subsequently suggested the same using first-principles calculations. Figure 4d illustrates the crystal structure of VO_2(B). The synthesis of VO_2(B) by a low-temperature solvothermal technique followed by blending with conductive reduced graphene oxide, rGO, forms the composite VO_2(B)/rGO. From the electrochemical testing, clearly VO_2(B)/rGO demonstrated a considerable enhanced performance compared to VO_2(B), as depicted in Figure 4e. Deng et al.[50] designed Mn-doped VO_2 (MnVO) to modify its electronic structure and thus improve the Zn^{2+} storage performance by doping in VO_2(B). This obtained material exhibits an excellent electrochemical performance at the current density of 5 A g^{-1}, with a capacity retention of 80.7% after 10,000 cycles. Cai et al.[51] also modified VO_2 by doping it with a Ni ion (NVO) as a cathode for AZIBs, which showed a high capacity of 182 mAh g^{-1} at 5 A g^{-1} and good cycling stability. The dopant effectively increases the kinetics of the NVO electrode by providing high surface reactivity and improving the intrinsic electronic configurations. Wang et al.[52] demonstrate that the boron at the intersitial site of VO_2(B) can boost the zinc storage kinetics and structural stability during cycling. Notably, the saturation limit of boron doping is 2 at. % which showed a high storage capacity of 281.7 mAh g^{-1} at 0.1 A g^{-1}.

Recently He et al.[53] showed that the electrode featuring dispersive (00*l*) facet-dominated VO_2(B) nanobelts displays directional and fast ion diffusion behavior exhibiting an ultrahigh-rate performance (420.8 and 344.8 mAh g^{-1} at 0.1 and 10 A g^{-1}, respectively) and long cycling stability (84.3% capacity retention for 5000 cycles at 10 A g^{-1}).

(*ii*) V_2O_3. V_2O_3 adopts a three-dimensional tunnel-like structure by sharing an edge with the next octahedron through two common VO_6 octahedra. The trigonal phase V_2O_3 ($R\bar{3}c$) exists as a 3D framework structure, and the tunnel facilitated the intercalation of cations.[54,55] Vanadium 3d electrons possess the ability to migrate along the V−V chain and often have superior electrical conductivity compared to most transition metal oxides.[56] The potential use of porous V_2O_3 pyrolyzed from vanadium-based MOF precursors as a cathode for AZIBs was initially demonstrated by Hu et al.[57] The CV plot depicted in Figure 5a illustrates the presence of two coupled redox peaks

https://doi.org/10.1021/acsomega.4c06199
ACS Omega 2024, 9, 47920−47938

at 0.92/1.04 and 0.56/0.72 V, indicating the presence of a two-step deinsertion/deinsertion process of Zn^{2+}. The specific capacity is determined as 300 mAh g^{-1} at 100 mA g^{-1}, as shown in Figure 5b. Additionally, a capacity retention of 90% post 4,000 cycles at 5 A g^{-1} (Figure 5c) accounts for exceptional cycling stability. The Zn^{2+} storage process was analyzed using *ex-situ* X-ray photoelectron spectroscopy (XPS), X-ray diffraction (XRD), and Raman experiments. During the discharge cycle, the migration of water molecules and Zn^{2+} into the tunnel structures of V_2O_3 occurred, resulting in their retention during the charge process. This phenomenon contributes to the expansion of the ion diffusion channel and the reduction of the Zn^{2+} diffusion resistance, as depicted in Figure 5d. The stability of the structure formed by the intercalated Zn^{2+} occupying the octahedral interstices of O atoms was further established using first-principles calculation, as illustrated in Figure 5e,f. Differential charge state density indicates the development of a chemical interaction between Zn^{2+} and O^{2-} originating from V_2O_3 (Figure 5g). The introduction of Zn^{2+} ions led to a decrease in the spatial separation and a profound interatomic contact, hence leading to the enhanced cycle stability of AZIBs. Nevertheless, the octahedral interstice size is insufficient to accommodate storage of multiple zinc ions, as evidenced by the related computational findings. Ding et al.[58] later determined that the presence of vanadium vacancies might enhance the process of Zn^{2+} intercalation/extraction. V_2O_3 with a high concentration of defects was synthesized by calcination of V_2O_5 in an NH_3/Ar environment by in situ electrochemical lattice conversion processes. The utilization of defect-rich V_2O_3 as the cathode resulted in a notable capacity of 382.5 mAh g^{-1} and an exceptional rate performance. During the initial charging step, the lattice structure of V_2O_3 underwent distortion, resulting in the formation of vanadium vacancies. These vacancies were advantageous for the succeeding cycles of Zn^{2+} de/intercalation. The activation of V_2O_3 through the formation of vanadium vacancies has the potential to accelerate the reaction kinetics of the AZIBs. However, the specific reaction mechanism remained unclear.

Recently, Wu et al.[59] synthesized a V_2O_3−VN nano-heterojunction composite with sea-urchin-like morphology and explored it as the cathode for AZIBs. The electrode achieves a capacity of 532.6 mAh g^{-1} at 0.1 A g^{-1} and 263.4 mAh g^{-1} at 5 A g^{-1} current density with 90.8% capacity retention. Chen et al.[60] showed the synthesis of V_2O_3 with a carbon shell (V_2O_3@C) by the reduction reaction of carbon with V_2O_5 in an oxygen-free environment and tested its electrochemical performance. Wang et al.[61] developed V_2O_3@C microspheres to achieve enhanced conductivity and improved stability of phase changes. Compounding vanadium oxides and conductive carbon through in situ carbonization led to a significant improvement of the cathode materials.

(*iii*) *V_2O_5*. V_2O_5 has the highest oxygen state in vanadium−oxygen systems and is the most stable member of the series of vanadium oxides. This compound exhibits a layered structure where vanadium and oxygen atoms arrange themselves in a square pyramidal shape, forming layers through coedges or cocorners,[62] with the layered orthorhombic V_2O_5 (*Pmnm*) structure. The adjacent layers are connected by van der Waals forces and hydrogen bonds between the layers with an interlayer spacing ∼0.58 nm, significantly exceeding the radius of Zn^{2+} (0.76 Å).[63] This facilitates the diffusion of Zn^{2+} between the V_2O_5 layers.[64] V_2O_5 undergoes a two-electron redox reaction and has the potential to store a significant amount of zinc, with a theoretical capacity of 589 mAh g^{-1} during the (dis)charge process.[65] Nevertheless, the significant polarization and volume fluctuation resulting from the incorporation of Zn^{2+} as a multivalent carrier into the cathode host continue to pose a significant challenge with superior performing AZIBs.[66] Furthermore, the low electrical conductivity of V_2O_5 poses a challenge to its widespread implementation.[67] To improve electronic conductivity, blending V_2O_5 with carbonaceous materials as nanotubes, nanofibers, and quantum dots (CQDs) led to a significantly improved electronic conductivity.[68−72] Zhang et al.[73] developed AZIBs using a ball-milled commercial V_2O_5 cathode, Zn anode, and a 3 mol L^{-1} $Zn(CF_3SO_3)_2$ electrolyte. The resulting AZIBs exhibited a reversible capacity of 470 mAh g^{-1} at 0.2 A g^{-1} (Figure 6a) and demonstrated a capacity retention of 91% over 4,000 cycles at 5 A g^{-1} (Figure 6b). Chen et al.[69] employed electrospinning technology to fabricate porous V_2O_5 nanofibers (Figure 6c) which exhibited a capacity of 319 mAh g^{-1} at 20 mA g^{-1} and a capacity retention of 81% over 500 cycles at 2 C (Figure 6d). The Zn^{2+} insertion/extraction process was elucidated using a two-step conversion mechanism, as depicted in Figure 6e, that involves the initial synthesis of open-structured zinc pyrovanadate ($Zn_{3+x}(OH)_2V_2O_7\cdot 2H_2O$) during the first discharge, followed by the reversible insertion/extraction of Zn^{2+} between $Zn_{3+x}(OH)_2V_2O_7\cdot 2H_2O$ and $Zn_{3+y}(OH)_2V_2O_7\cdot 2H_2O$.

Javed et al.[70] grew 2D V_2O_5 nonagglomerated nanosheets on a Ti substrate to increase the interaction between V_2O_5 and the collector. The resulting cathode demonstrated a discharge capacity of 503.1 mAh g^{-1} at a current density of 100 mA g^{-1}, along with long-term stability (86% retention over 700 cycles at a current density of 500 mA g^{-1}). Recently, Linghua et al.[74] synthesized porous V_2O_5 slender leaf-like nanostructures anchored on carbon cloth (CC) via electrodeposition and subsequent calcination. Taking advantage of the distinctive hierarchical structure and the introduction of propylene carbonate (PC) electrolyte additives, the free-standing composite electrode provided a maximum reversible capacity of 555 mAh g^{-1} at 0.3 A g^{-1} and high-capacity retention of 180 mAh g^{-1} after 5000 cycles at 10 A g^{-1}. Zafar et al.[75] developed an approach to create a layer-separated V_2O_5 ultrathin nanosheet (expanded 1.21 nm) composite cathode material. This distinctive hybrid structure resulted in a high capacity of 515 mA h g^{-1} at 0.1 A g^{-1} and stability over 2000 cycles at 3 A g^{-1}.

Li et al.[76] reported a hydrothermal method for the preparation of chitosan-derived carbon dots (CCDs) in V_2O_5 nanobelts, CCDs@V_2O_5. The unique one-dimensional structure of CCDs@ V_2O_5 nanobelts exhibited a specific capacity of 401.4 mAh g^{-1} at the current density of 0.1 A g^{-1}. After cycling for 400 cycles at 1 A g^{-1}, the specific capacity remains at 285.3 mAh g^{-1}. After 2000 cycles at 4 A g^{-1}, the specific capacity still reaches 212.30 mAh g^{-1} with a capacity retention rate of 83.77%. Jia et al.[77] synthesized MIL-88B(V)@rGO composites, in which MIL-88B(V) nanorods are anchored on reduced graphene oxide (rGO) sheets, as cathodes for ZIBs. During the initial charge/discharge process, the cathode undergoes an in situ irreversible transformation from MIL-88B(V) to amorphous V_2O_5 that acts as an active site for the subsequent Zn^{2+} insertion/extraction.

3.2. Introduction of Vanadates in AZIBs. Vanadates possess a high concentration of vanadium and V−O polyhedra

https://doi.org/10.1021/acsomega.4c06199
ACS Omega 2024, 9, 47920−47938

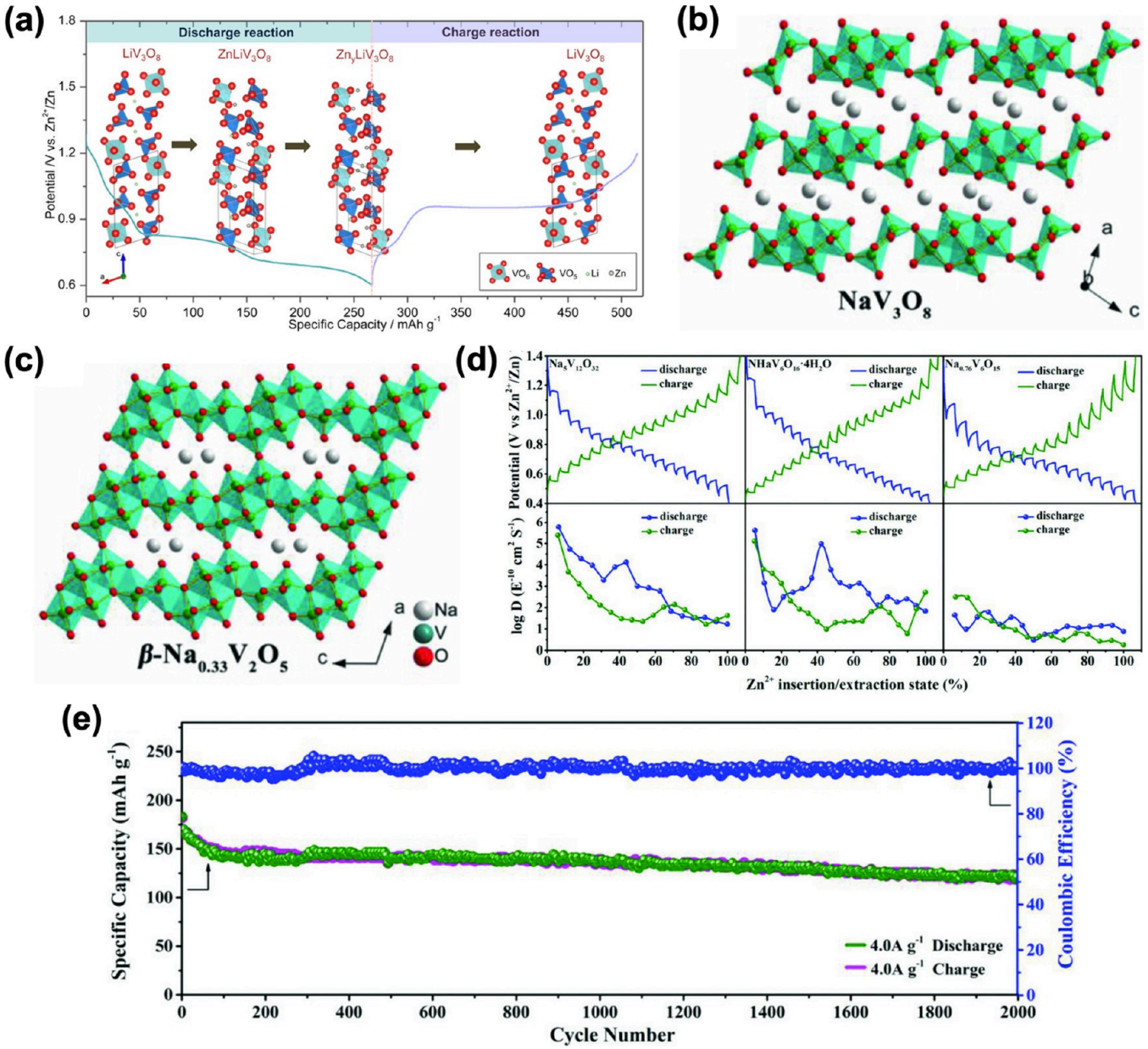

Figure 7. (a) Schematic of the Zn-intercalation mechanism in the LiV_3O_8 cathode. Reproduced with permission from ref 80. Copyright 2017, American Chemical Society. The crystal structure of (b) NaV_3O_8, (c) β-$Na_{0.33}V_2O_5$, and (d) GITT curves and the corresponding Zn_{2+} diffusion coefficient of $Na_5V_{12}O_{32}$, $HNaV_6O_{16}{\cdot}4H_2O$, and $Na_{0.76}V_6O_{15}$. (e) Long-term cycling performance at 4 A g^{-1} of $Na_5V_{12}O_{32}$. Reproduced with permission from ref 82. Copyright 2018, Wiley-VCH.

and can be easily deformed. In general, the synthesis of vanadates involves the intercalation of vanadate oxides with various types of cations. The intercalating cations potentially enhance the internal spacing of vanadium oxides, thus mitigating the capacity loss experienced by these oxides. Furthermore, incorporation of cations into the material results in a "pillar effect", which stabilizes the layered structure and prevents "lattice respiration", ultimately.[78,79] A diverse range of metal ions, such as monovalent alkali metal cations (e.g., Li^+, Na^+, K^+), multivalent alkali metal cations (e.g., Ca^{2+}, Mg^{2+}), transition metal cations (e.g., Cu^{2+}, Ag^+), and nonmetal cations (e.g., NH_4^+), are reported to intercalate within layers of vanadium oxides. It is often used to modify the properties of materials, such as conductivity, mechanical strength, or chemical reactivity. Likewise, the intercalation of water molecules as hydrated vanadates offers distinctive characteristics.

3.2.1. Monovalent Alkali Metal-Cation-Based Vanadates. Layered V_3O_8 compounds, namely, LiV_3O_8, NaV_3O_8, and KV_3O_8, have been identified as potential alternatives for the storage of Zn^{2+} ions. Among these, LiV_3O_8 stands out because the ease of synthesis and layered structure allows fast ion diffusion, leading to a notable capacity of Zn/LiV_3O_8 batteries. The electrochemical reaction process (Figure 7a) is presented as follows.

Anode:

$$Zn \rightarrow Zn^{2+} + 2e^-$$

Cathode:

https://doi.org/10.1021/acsomega.4c06199
ACS Omega 2024, 9, 47920−47938

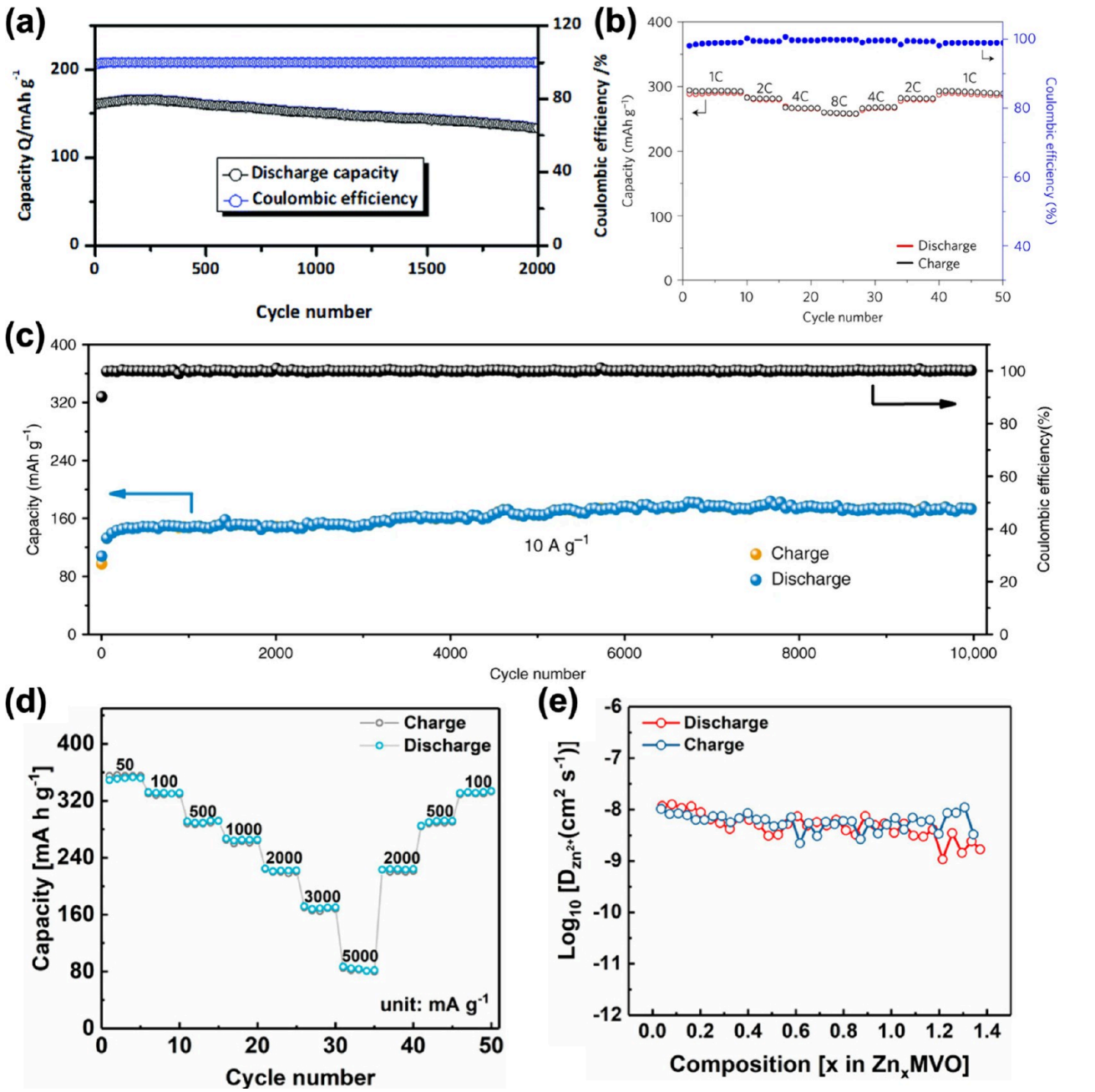

Figure 8. (a) Long-term cycling performance of the BDHS sample. Reproduced with permission from ref 86. (b) Rate capability at varying C rates and the corresponding Coulombic efficiencies. Reproduced with permission from ref 2. Copyright 2016, Springer Nature. (c) Cycle performance of $CaV_6O_{16}{\cdot}3H_2O$ at 10 A g^{-1}. Reproduced with permission from ref 88. Copyright 2020, Springer Nature. (d) Rate performance of the $Mg_{0.34}V_2O_5{\cdot}0.84H_2O$/Zn cell. (e) The zinc ion diffusion coefficient of the $Mg_{0.34}V_2O_5{\cdot}0.84H_2O$ cathode. Reproduced with permission from ref 89. Copyright 2018, American Chemical Society.

$$yZn^{2+} + LiV_3O_8 \rightarrow Zn_yLiV_3O_8$$

Zn^{2+} intercalates to the $ZnLiV_3O_8$ phase initially, followed by the formation of the reversible solid solution $Zn_yLiV_3O_8$ ($y > 1$) phase. During the process of charging, the newly formed phase undergoes a conversion back to LiV_3O_8.[80] Additionally, the high solubility of the LiV_3O_8 cathode in $ZnSO_4$ electrolyte deteriorates cycling performance, which is inferior to that of vanadium oxide even though V^{5+} exists in a state of high oxidation. The theoretical capacity of this two-electron transfer reaction can reach 560 mAh g^{-1}, based on the quantitative conversion of V^{5+} to V^{3+}. He et al.[81] devised a mechanism for a bielectron transfer process, with the capability to effectively suppress the volume expansion during intercalation through a phase transition between α-$Zn_xLiV_3O_8$ ($x < 2$) and β-$Zn_yLiV_3O_8$ ($2 \leq y \leq 3$). This phase transition results in a capacity of 557.5 mAh g^{-1} and maintains a capacity retention of 85% over 4000 cycles. The utilization of the V^{5+}/V^{3+} double redox method in this study has significant advantages in enhancing the electrochemical performance and presents a novel avenue for the development of cathode materials in ZIBs.

Likewise, the crystal structure of NaV_3O_8 closely resembles that of LiV_3O_8 with a V_3O_8 polyhedron and Na^+ ions positioned between the layers of octahedral sites as in

https://doi.org/10.1021/acsomega.4c06199
ACS Omega 2024, 9, 47920−47938

$Na_5V_{12}O_{32}$ and $HNaV_6O_{16}\cdot 4H_2O$. The tunnel-like structure, depicted in Figure 7b,c, consists of an octahedron (VO_6) and a square cone (VO_5) that share sides. Within this structure, a single oxygen atom is shared to create a tunnel along the *b* axis and Na^+ insertion resulting in the formation of tunnel-type *β*-$Na_{0.33}V_2O_5$ (e.g., $Na_{0.76}V_6O_{15}$). The nanowires of $Na_{0.33}V_2O_5$ showed a capacity of 367.1 mAh g^{-1} at 0.1 A g^{-1} and demonstrated cycling stability with a retention rate of 93% after 1000 cycles. This can be attributed to their favorable conductivity and stable crystal structure.[83] The layered structure offers a more efficient pathway for the diffusion of Zn^{2+} in comparison to the tunnel type structure. The ion diffusion coefficient of $Na_5V_{12}O_{32}$ and $HNaV_6O_{16}\cdot 4H_2O$ compounds is higher compared to $Na_{0.76}V_6O_{15}$ (Figure 7d). This can be attributed to the significant lattice spacing of the two-dimensional layered structures. Furthermore, the Zn/$Na_5V_{12}O_{32}$ battery exhibits an exceptionally extended cycle life, with a capacity retention of 71%, as depicted in Figure 7e.[82]

Furthermore, potassium vanadate exhibits diverse crystal structures. The findings indicate that layered KV_3O_8 and $K_2V_6O_{16}$, $K_2V_8O_{21}$, and $K_{0.25}V_2O_5$, which possess a tunnel structure, exhibit enhanced structural stability. This characteristic allows for the prevention of structural collapse during continuous charging and discharging cycles. Due to the larger ion radius of potassium than sodium, the presence of K^+ in tunnel structural materials can effectively regulate charge balance, enhance structural stability, and increase the storage capacity of Zn^{2+}.[84]

3.2.2. Multivalent Alkali Metal-Cation-Based Vanadate. Theoretically, a rechargeable battery containing multivalent ions has the potential to offer substantial storage capacity as a result of numerous electron exchanges. The Kim group reported facile hydrothermal synthesis of one-dimensional $Zn_2V_2O_7$ nanowires with a layer structure. The cell composed of Zn/$Zn_2V_2O_7$ exhibits notable rate durability and possesses an energy density of 114 Wh kg^{-1}.[85] Nevertheless, developing innovative electrode structures is crucial to enhancing the overall performance of the cells. Zhou et al.[86] employed a double template formation technique to synthesize bubble-encapsulated double-shelled $Zn_2V_2O_7$ hollow spheres (BDHSs). The distinctive structure offers a highly porous framework and numerous active sites, thereby augmenting electrochemical kinetics and attaining a rather consistent cycle life with a capacity attenuation of 16.9% after 2000 cycles (Figure 8a). In addition to $Zn_2V_2O_7$ materials, hydrated V_2O_5 derivatives ($Zn_{0.25}V_2O_5\cdot nH_2O$), which possess the open structure of V_2O_5 electrodes, were also investigated. HRTEM images demonstrate that the lattice spacing of 0.537 nm aligns with the (200) plane, and the crystal exhibits growth along the *b* axis. Furthermore, water inclusion allowed acquisition of a capacity of 282 mAh g^{-1} (Figure 8b).[2]

Xia et al.[87] recently demonstrated the synthesis of double-layered $Ca_{0.25}V_2O_5\cdot nH_2O$ nanobelts. The longer Ca−O bond length than Zn−O resulted in a larger interlayer gap in the former. A 4-fold higher conductivity of $Ca_{0.25}V_2O_5\cdot nH_2O$ than $Zn_{0.25}V_2O_5\cdot nH_2O$ led to the enhanced efficiency of Zn^{2+} transfer during the charge and discharge mechanism. Consequently, the cell maintains a capacity of 96% even after 3000 cycles and an energy density of 267 Wh kg^{-1}. Niu et al.[88] introduced a self-charging system that utilizes $CaV_6O_{16}\cdot 3H_2O$ cathodes and employs a redox reaction system in an oxygen-rich environment. The capacity of 170 mAh g^{-1} exhibited stability even after 10,000 cycles at a current density of 10 A g^{-1}, as depicted in Figure 8c.

Alshareef et al.[89] proposed that the Mg^{2+} intercalated V_2O_5 ($Mg_{0.34}V_2O_5\cdot 0.84H_2O$) cathode showcased a broad potential range of 0.1−1.8 V with the rate performance of 353 mAh g^{-1}@50 mA g^{-1} and 81 mAh g^{-1}@5000 mA g^{-1}, as shown in Figure 8d. Based on the GITT calculations, the diffusion coefficient of $Mg_{0.34}V_2O_5\cdot 0.84H_2O$ was determined as 10^{-8}∼10^{-9} cm^{-2} s^{-1} (Figure 8e), which is significantly higher than bare V_2O_5. The nanobelt and porous structure of $Mg_{0.34}V_2O_5\cdot 0.84H_2O$ demonstrated the ability to facilitate the swift movement of Zn^{2+} ions due to preintercalation of Mg^{2+} ions favoring high-rate performance. Ex-situ XRD studies revealed that the majority of Mg^{2+} ions were substituted by zinc ions after the initial cycle to form $Zn_{0.3}Mg_xV_2O_5$, which further served as the host cathode for subsequent cycles. It consists of two distinct solid solutions, $0.8 > x > 0$ and $1.4 > x > 0.8$. Upon reaching a voltage of $x \sim 0.8$ (1.8−0.8 V) during the process of discharge, a slight reduction in the gap between layers is observed as indicated by the displacement of the diffraction peaks toward higher angles. The interlayer electrostatic repulsion is masked by the structural water (solvation effect) when Zn^{2+} is added, as the zinc ion content increases. Moreover, the formation of hydrogen bonds during the reaction resulted in the convergence of the bilayers. In addition, the development of a novel phase was also seen during the release process at voltages ranging from 0.6 to 0.3 V. The material indicated that the new phase is layered $Zn_{(z+0.3)}Mg_xV_2O_5$, based on the equal spacing of the diffraction peaks, where $1.4 > 0.8$. The data indicate that the energy storage process can be categorized into two distinct phases: the first cathode cycle and the subsequent cathode cycle. The overall reaction after the first cycle is described as

$$Zn_{0.3}Mg_xV_2O_5 + zZn \leftrightarrow Zn_{(z+0.3)}Mg_xV_2O_5$$

In addition to the aqueous environment, Chen et al.[90] also conducted an evaluation of the utilization of $Mg_{0.19}V_2O_5\cdot 0.99H_2O$ in a quasi-solid-state zinc−ion battery. The battery showed remarkable versatility under diverse severe situations. In contrast to the previously stated $Mg_xV_2O_5\cdot nH_2O$ cathode, a more recent development is the introduction of a two-dimensional $Mg_{0.2}V_2O_5\cdot nH_2O$ nanobelt cathode by Sun et al.[91] This cathode exhibits a mechanism for the insertion and removal of Zn^{2+} and H^+ ions. The conductive V_4C_3 MXenes served as the cathode, while the aqueous ZIBs and soft pack batteries exhibited exceptional electrochemical characteristics. The enhanced performance can be attributed to, namely, the capacity of the hydrated ions synthesized by Mg^{2+} and structural water to maintain the integrity of the layered structure and facilitate the movement of ions and electrons between the layers of V_2O_5. Recently, the alkaline earth metal elements Ca^{2+}, Mg^{2+}, and Sr^{2+} have been explored as an intercalant for V_2O_5, expanding the galleries.[92]

Understanding the intricate Zn^{2+} storage mechanism is vital to achieve the aim of establishing a high-performing water-based AZIB system and find solutions for challenges like irreversible byproducts [$Zn_4SO_4(OH)_6\cdot xH_2O$] and dissolution of vanadium-based compounds into the electrolyte.[93,94] To mitigate these issues, Xiong et al.[95] explored barium vanadate, specifically $Ba_{1.2}V_6O_{16}\cdot 3H_2O$, $BaV_6O_{16}\cdot 3H_2O$ of V_3O_8-type, and $Ba_xV_2O_5\cdot nH_2O$ of V_2O_5-type, which exhibited no observable alteration in color for a prolonged duration of 3600 h and retained the phase structure even after 1000 cycles.

https://doi.org/10.1021/acsomega.4c06199
ACS Omega 2024, 9, 47920−47938

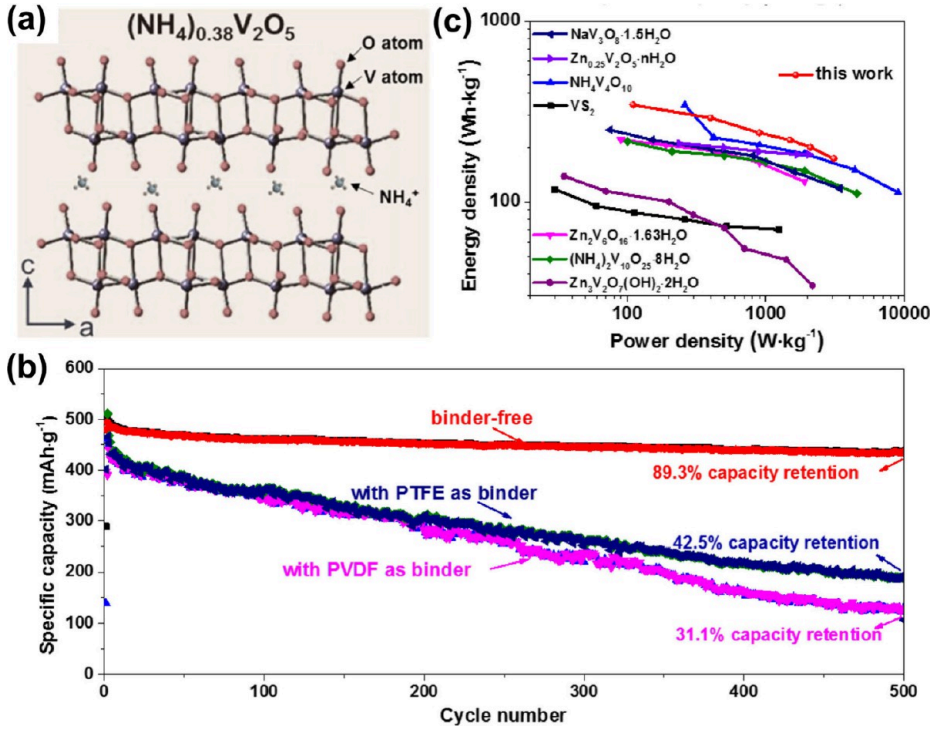

Figure 9. (a) Atomic structure of layered $(NH_4)_{0.38}V_2O_5$ crystal. (b) Ragone plots of $(NH_4)_{0.38}V_2O_5$/CNT paper electrode compared to other cathodes for AZIBs. (c) The cycle performance comparison between the $(NH_4)_{0.38}V_2O_5$/CNT paper electrode and the control electrode prepared through slurring with PVDF/PTFE as binder. (a–c) Reproduced with permission from ref 100. Copyright 2021, Elsevier.

In other work, the reduction displacement reaction (RDR) mechanism was initially proposed by Shan et al.[96] for the Zn/$Cu_3(OH)_2V_2O_7·2H_2O$ battery. The presence/disappearance of Cu^0 and the new phase $Zn_{0.25}V_2O_5·H_2O$ throughout the discharge/charge process was confirmed using ex-situ XRD and XPS experiments. This procedure demonstrates a highly reversible reaction. The RDR mechanism is evident, where the process demonstrates the substitution of Cu^{2+} with $Zn_{0.25}V_2O_5·H_2O$ and the reduction of Cu^{2+} to Cu. The Zn/$Cu_3(OH)_2V_2O_7·2H_2O$ system exhibited a specific capacity of 336 mAh g^{-1} at 1 A g^{-1} and maintained its capacity of 136 mAh g^{-1} after 3000 cycles, which is attributed to its improved reaction mechanism.

3.2.3. Nonmetal Cation-Based Vanadate. A stable bilayer structure is formed by the monoclinic $(NH_4)_{0.38}V_2O_5$ unit structure, which is composed of deformed VO_6 octahedrons with shared edges (Figure 9a). The octahedral oxygen atoms exhibit robust interactions with NH_4^+ ions. These cations function as "pillars" to stabilize the structure and mitigate volume fluctuations in the interlayer spacing with the entry/exit of ions.[97] Furthermore, when compared to other vanadium cations like sodium and potassium, ammonium cations demonstrate comparatively lower molecular weight and density while also offering higher specific gravity and volumetric capacity.[98,99]

Jiang et al.[100] demonstrated the inherent knitting characteristics of thin and flexible $(NH_4)_{0.38}V_2O_5$ nanoribbons and explored them as binder-free paper cathodes. Incorporation of carbon nanotubes (CNTs) improved the electrical conductivity and created a porous structure, leading to an initial specific capacity of 465 mAh g^{-1}, which remains at 89.3% after 500 cycles at the rate of 0.1 A g^{-1} (Figure 9b). Furthermore, it can be observed from Figure 9c that the paper cathode exhibits a specific energy of up to 343 Wh kg^{-1}, surpassing the performance of most of the ZIBs with polymer binders.[101−105] The existence of large size NH_4^+ (1.43 Å) and H_2O (4 Å) in the interstitial space of $NH_4V_3O_8·0.5H_2O$ theoretically enables the reversible insertion and removal of Zn^{2+} (0.74 Å) while also accommodating volume expansion.[106] In V_3O_8-type materials, an increase in water molecules such as $(NH_4)_2V_6O_{16}·1.5H_2O$ enhances the electrochemical performance.[107] Additionally, ammonium vanadates exhibit a low molecular weight, resulting in a significant capacity for volume storage.

3.3. Polyanionic Compounds. Polyanionic compounds are known for their stable frameworks and high operating voltage, and substantial research using them as cathode materials in monovalent metal−ion batteries is explored.[108] The polyanion-type compounds consist of polyhedra formed by corner- and/or edge-sharing MO_x (where M represents transition metals such as V, Mn, Cr, Fe, Ti, Co, etc.) and tetrahedra anion groups consisting of $(XO_4)_m^{n-}$ or $X_m(O_{3m+1})^{n-}$ (where X represents nonmetals such as P, S, B, Si, etc.). The strong covalent bonds between oxygen atoms with the M and X crystal frameworks of polyanion-type are robust and exhibit excellent thermal stability. Additionally, this prevents the release of O_2 and protects deterioration in performance at high current density.[109] In addition, polyanionic cathodes typically exhibit elevated redox potentials due to the distinctive "inductive effect", associated with the alterations in molecular orbitals produced as a result of polyanion $(XO_4)^{n-}$ or $X_m(O_{3m+1})^{n-}$ groups. However, only few research papers document their ability to comprehend the reversible Zn−ion intercalation chemistry. Additionally, many of these materials have limited ability to hold a large number of Zn ions due to their high molecular weights and restricted structures; however, their potential for providing high redox potentials is promising. For instance, the strong inductive effect caused by

https://doi.org/10.1021/acsomega.4c06199
ACS Omega 2024, 9, 47920−47938

Table 1. Electrochemical Performance of Various V-Based Materials As a Cathode for Aqueous ZIBs

Cathodic materials	Electrolyte	Capacity (mAh g^{-1}) at current density (A g^{-1})	Capacity retention (%) (cycles)	References
V_2O_5	$Zn(CF_3SO_3)_2$	470 (0.2)	91.1% (4000)	73
V_2O_3	$ZnSO_4$	207 (0.1)	82.1% (2500)	126
V_2O_3@C	$Zn(CF_3SO_3)_2$	350 (0.1)	90% (4000)	57
a-V_2O_5	$Zn(CF_3SO_3)_2$	348 (0.1)		127
V_2O_5/YS	$Zn(CF_3SO_3)_2$	410 (0.1)	80% (1000)	128
V_2O_5/CNT	$ZnSO_4$	312	81% (2000)	129
C@V_2O_5	$Zn(CF_3SO_3)_2$	361 (0.5)	71% (2000)	130
VO_2	$Zn(CF_3SO_3)_2$	274	79% (10000)	131
$Na_{0.33}V_2O_5$	$Zn(CF_3SO_3)_2$	367.1 (0.1)	96% (1000)	83
$Na_{1.1}V_3O_{7.9}$@rGO	$Zn(CF_3SO_3)_2$	220 (0.3)		132
$Li_xV_2O_5{\cdot}nH_2O$	$ZnSO_4$	192 (10)	96.1% (800)	133
$Ca_{0.67}V_8O_{20}{\cdot}3.5H_2O$	$Zn(CF_3SO_3)_2$	466 (0.1)	95% (1000)	134
$Ag_2V_4O_{11}$	$Zn(CF_3SO_3)_2$	213 (0.2)	93% (6000)	135
$K_{0.5}V_2O_5$	$ZnSO_4$	150 (5)	75% (3000)	136
CuV_2O_6	$Zn(CF_3SO_3)_2$	338 (0.1)	100% (1200)	137
LiV_3O_8	$Zn(CF_3SO_3)_2$	557.5	95% (4000)	81
CaVOH/rGO	$Zn(CF_3SO_3)_2$	409 (0.05)	90% (2000)	138
$Zn_3V_3O_8$	$Zn(CF_3SO_3)_2$	285 (0.15)	72.6% (2000)	139
SrVO/CNT	$Zn(CF_3SO_3)_2$	326 (0.1)	91% (7500)	92
$Na_7V_{7.6}O_{20}{\cdot}4H_2O$	$Zn(CF_3SO_3)_2$	309.4 (0.3)	98.6% (10000)	140
$Zn_{0.1}V_2O_5{\cdot}nH_2O$	$ZnSO_4$	463 (0.2)	88% (20000)	141
$(NH_4)_{0.5}V_2O_5$	$ZnSO_4$	418.4 (0.1)	91.4% (2000)	142
$Na_3V_2(PO_4)_2F_3$	$Zn(CF_3SO_3)_2$	61.7	95% (4000)	143

the P−O bonds in the $(PO_4)^{3-}$ groups benefits their usage as high-energy-density cathodes.

NASICON-type cathode materials have a stable framework that is advantageous for a long-term cycle life. The redox potential of these materials is higher than that of V-based oxides and many organic compounds due to the strong inductive effect of polyanionic groups. Additionally, their structure contains numerous vacancies to store metal ions. $Na_3V_2(PO_4)_3$ has been thoroughly researched as cathode material with a NASICON-type structure in sodium−ion batteries (SIBs).[110] The Huang group first developed a carbon wrapped $Na_3V_2(PO_4)_3$ that resembled graphene and explored it as a cathode in AZIB. The NASICON-$Na_3V_2(PO_4)_3$ framework demonstrated exceptional Zn^{2+} storage capacity, resulting in the Zn−$Na_3V_2(PO_4)_3$ battery exhibiting remarkable performance in terms of both rate and cycling. It achieved a reversible capacity of 97 mA h g^{-1} at 0.5 C and maintained a capacity retention of 74% after 100 cycles.[111] Inspired by this work, many investigations of NASICON type cathode materials have been reported. In 2018, a study showcased the use of fluorophosphate vanadium-based materials by incorporating an intercalated $Na_3V_2(PO_4)_2F_3$ cathode with a carbon-film-functionalized Zn(CFF-Zn) anode and Zn-$(CF_3SO_3)_2$ as an electrolyte.[112] The aqueous Zn/$Na_3V_2(PO_4)_2F_3$@C battery exhibited a much greater voltage output of 1.62 V compared to the $Na_3V_2(PO_4)_3$ cathode. A charge capacity of 75 mAh g^{-1} was initially recorded during the first charging step, during which Na^+ ions are extracted. Subsequently, the capacities marginally dropped as Zn^{2+} ions participated. Recently, $Na_3V_2(PO_4)_2F_3$@rGO showed a capacity of 126.9 mAh g^{-1} at 0.5 C (1 C = 128 mA g^{-1}), redox potentials at 1.48/1.57 V, and cycling stability with capacity decay of 0.0074% per cycle after 5000 cycles at 15 C.[113]

Layered $VOPO_4$ and its hydrates, among other types of polyanionic compounds, have also been investigated as hosts for Zn^{2+}. Wang et al.[114] examined the effect of water in $Zn(OTf)_2$ electrolyte on the ability of a $VOPO_4$ cathode to store Zn ions. With the inclusion of water (1%), the movement of water from the electrolyte to the host lattice led to an enhanced diffusion of Zn^{2+} at the interface between the electrolyte and electrode, resulting in a significant rise in capacity. Nevertheless, the primary challenge in advancing ZIBs lies in the absence of appropriate robust hosts capable of accommodating Zn^{2+} ions that experience significant electrostatic repulsion. Investigating Zn-storage cathode materials with low-strain properties is an essential approach to tackling the issues. Recently, a layered phyllo-oxovanadophosphate $Zn_{0.56}VOPO_4{\cdot}2H_2O$ as a structurally stable cathode material developed a tiny lattice volume distortion of 1.9%, high operating voltage of 1.46 V, and ultralong cycle life (capacity retention of 70.5% after 8000 cycles).[115]

3.4. Oxygen-Free Vanadium-Based Compound. Vanadium disulfide (VS_2) is classified as a transition metal dichalcogenide with a distinctive chain-layered structure, resembling graphite. In VS_2, the V and S atoms are chemically bound together, and the neighboring layers (S−V−S) are held together by a weak van der Waals interaction, with a high interlayer spacing of 0.58 nm facilitating the storage of Zn^{2+}, Al^{3+}, and Mg^{2+} as guests.[116,117] He et al.[118] initially examined the process by which Zn^{2+} is inserted into VS_2 nanosheets. During the discharge procedure, the phase transitions from VS_2 to $Zn_{0.09}VS_2$ and subsequently to $Zn_{0.23}VS_2$ took place within a voltage range of 0.65−0.82 V and 0.45−0.65 V, respectively. The increase in the interlayer of VS_2 along (002) following the insertion of Zn^{2+} is merely 1.73%. VS_2 cathode based AZIBs showed a reversible specific capacity of 190.3 mAh g^{-1} at 0.05 A g^{-1} within 0.4−1.0 V, and an initial capacity retention rate achieved 98% after 200 cycles at 0.5 A g^{-1}. However, the poor energy density of VS_2 was due to the small voltage window (0.4−1.0 V vs Zn^{2+}/Zn). Recently, Zafar et al.[119] developed a facile method to fabricate quasi-solid-state supercapacitors

https://doi.org/10.1021/acsomega.4c06199
ACS Omega 2024, 9, 47920−47938

(QSSCs) and ZIBs using the PANI/VS_2 composite. The conductivity and charge acceptor properties improved due to networks of PANI on the layered VS_2 accounting for a charge storage capacity of 219 mA h g^{-1} at a discharge rate of 0.1 A g^{-1}. It demonstrated a Coulombic efficiency of 100% after 750 continuous cycles at 3 A g^{-1}.

A structural analogue to VS_2, monoclinic VS_4 ($I2/c$) is a distinctive one-dimensional atomic chain composed of V^{4+} ions coupled to sulfur dimers (S_2^{2-}) with a interlayer space bigger (0.583 nm) than VS_2.[120−122] The VS_4@rGO composite exhibited a capacity of 180 mAh g^{-1} at 1 A g^{-1} for 165 cycles, with a capacity retention rate of 93.3%.[123] Rong et al.[124] reported the synthesis of highly stable vanadium nitride (VN) particles. Benefiting from the small particle size and porous stacked structure, VN showed a capacity of 496 mAh g^{-1} at 0.1 A g^{-1} and stable capacity of 82 mAh g^{-1} after 8000 cycles. Yao et al.[125] architected vanadium nitride nanosheets over titanium-based hollow nanoarray skeletal hosts to modulate its properties by creating multiple interfaces and maintaining the phase of VN. Benefiting from the modulated crystalline thermodynamics during the electrochemical activation of VN, it demonstrates remarkable discharge capacities of 802.5 and 331.8 mAh g^{-1} at 0.5 and 6.0 A g^{-1}.

As we all know, the crystal structure and morphology of electrodes and various electrolytes can exert an important impact on the electrochemical performance of the battery system. The common issues of AZIBs based on V-based compounds are a low operating voltage and poor electrode conductivity. To overcome these challenges, using a simple approach, cathode materials are modified by inclusion of water molecules, doping metal ions, and blending with conductive materials. Fortunately, these strategies are effective to improve the specific capacity and cycle stability for vanadium-based materials. Table 1 summarizes the electrochemical performances of some vanadium-based materials.

4. STRATEGIES FOR STABLE VANADIUM-BASED MATERIALS

4.1. Guest Preintercalation. Incorporating interlayer substances (such as cations, water molecules, or polymers) as structural pillars is a widely adopted method to address the issues of narrow interlayer spacing and instability in cathodes. This strategy is effective because many of these intercalated species can significantly increase lattice spacing.[65,87] Additionally, the presence of structural water can shield the Zn^{2+} charge, reducing electrostatic interactions and thereby enhancing the diffusion properties of Zn^{2+} ions both kinetically and thermodynamically, which contributes to an extended lifespan of the cathode.[144] However, not all intercalated cations can achieve this effect; for example, vanadates incorporated with K^+ exhibit high stability but with reduced lattice spacing. Thus, it is crucial to explore mechanisms beyond mere interlayer spacing adjustment, considering the ionic character of chemical bonds.

4.2. Defect Engineering. To modulate the electronic and ionic conductivity properties, defect engineering—such as elemental doping and the introduction of vacancies—is a well-explored approach. Cation doping enhances chemical bonding, facilitates cation ordering, and improves the electrical conductivity of the host material, which lowers the energy barrier for ion diffusion and thus supports rapid kinetics and long-term cycling stability.

In cases where strong electrostatic interactions exist between oxygen atoms and Zn^{2+} ions, introducing oxygen defects into the lattice can help mitigate Zn^{2+} ion capture, leading to stable cycling performance even under deep discharge/charge conditions. Conversely, vanadium (V) vacancies increase the number of reactive sites by directly storing Zn^{2+} ions and facilitate Zn^{2+} diffusion with minimal electrostatic repulsion, leading to improved transfer kinetics as evidenced by reduced Zn^{2+} intercalation energies. However, the precise characterization and controlled fabrication of these defects remain challenging. Recent advancements have allowed researchers to determine the concentration and spatial distribution of V defects by using advanced characterization techniques. It has been observed that during the initial discharge Zn^{2+} ions preferentially occupy V vacancy sites and are partially anchored to these vacancies, indicating a self-optimization process.

4.3. Electronic Conductivity Enhancement. Driven by the need to enhance electronic conductivity, researchers have extensively focused on developing composites by integrating vanadium-based materials with substances that exhibit high electrical conductivity.[145] Another approach involves fabricating binder-free cathodes by directly growing active materials onto current collectors.[70] Binder-free cathodes offer numerous exposed reactive sites and facilitate rapid charge transport kinetics, making them promising for applications in flexible devices. However, the current technology for preparing binder-free cathodes is not yet sufficiently advanced for practical use. Additionally, the presence of mixed valence states in vanadium compounds can enhance electronic conductivity through electron hopping between different valence states of vanadium.[42]

4.4. Electrolyte Optimization. In electrolytes, water exists in two forms: free and solvated due to the solvation process. The presence of active water weakens the H−O bonds, enhancing the likelihood of deprotonation and hydrolysis, which can lead to the formation of byproducts. Additionally, active free water can interact with the active materials, causing significant dissolution of the cathode. Therefore, optimizing electrolytes is primarily guided by two principles: (i) minimizing the amount of active free water and (ii) regulating the dissolution equilibrium to stabilize the electrolyte structure.

5. ELECTROLYTES

The selection of electrolyte employed within a battery cell significantly influences its electrochemical performance, as it is intimately linked to the reactions involving the extraction and reintroduction of active ions at the cathode. It has been well established that one of the principal advantages of ZIBs is their compatibility with a diverse range of electrolytes, both aqueous and organic, owing to their extensive pH tolerance (pH: 3.6−6.0). This broad pH range permits the use of various compatible solutions, allowing researchers to choose based on specific needs. Typically, ZIBs employ electrolytes with neutral or mildly acidic pH values, as alkaline conditions promote dendrite formation, and highly acidic electrolytes are susceptible to hydrogen gas evolution. Historically, KOH electrolytes were utilized in zinc primary batteries, but due to their propensity to induce anodic dendrite formation in secondary batteries, there has been a shift toward nonalkaline alternatives. To date, a variety of zinc salts have been documented, including $ZnSO_4$, $Zn(NO_3)_2$, $ZnCl_2$, $Zn(ClO_4)_2$, ZnF_2, $Zn(CF_3SO_3)_2$, $Zn(TFSI)_2$, and $Zn(CH_3COO)_2$, among others. Notably, NO_3^- anions act as potent oxidizing agents,

https://doi.org/10.1021/acsomega.4c06199
ACS Omega 2024, 9, 47920−47938

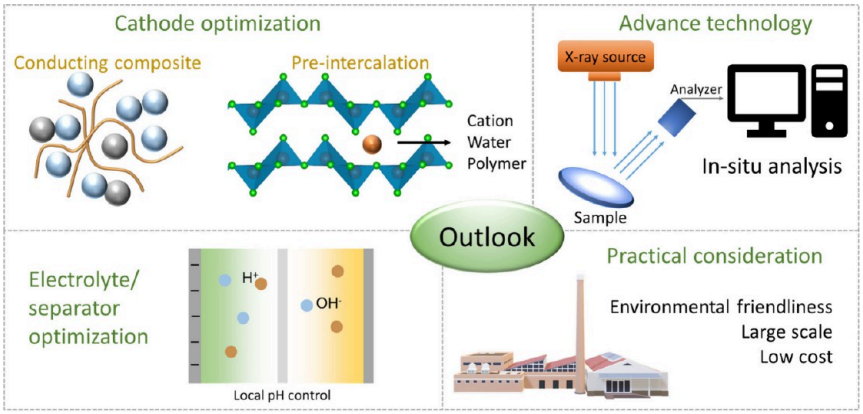

Figure 10. Outlook for stable vanadium-based aqueous zinc−ion batteries.

capable of oxidizing the zinc foil, which leads to significant corrosion of the zinc foil and a pronounced increase in both local pH and the overall electrolyte system.[146] ClO_4^- anions can alleviate zinc anode corrosion; however, their interaction with Zn^{2+} ions may lead to the formation of a ZnO passivation layer on the anode, thereby increasing the barrier to Zn^{2+} dissolution and deposition and slowing the reaction kinetics. Due to the low oxidation potential of Cl^- ions, $ZnCl_2$ is a feasible electrolyte for ZIBs. Nonetheless, its narrow anodic potential window leads to ongoing electrolyte decomposition at higher voltages, which constrains its practical utility.

In contrast, $ZnSO_4$ is the most commonly utilized electrolyte due to the stable nature of SO_4^{2-} anions and their excellent compatibility with the zinc anode.[147,148] Despite this, $ZnSO_4$ still encounters challenges such as hydrogen evolution and byproduct formation, which adversely affect the Coulombic efficiency of zinc stripping and plating and impede further development. Recently, it has been observed that the organic zinc salt $Zn(CF_3SO_3)_2$, which contains large CF_3SO^{3-} anions, can enhance electrolyte performance compared to SO_4^{2-} (which has a double charge). This improvement is attributed to the reduction in the number of water molecules surrounding Zn^{2+} ions, decreased solvent effects, and the release of Zn^{2+} ions from a tightly bound solvation sheath. These factors collectively facilitate better Zn^{2+} ion migration and increased charge-transfer rates. Consequently, $Zn(CF_3SO_3)_2$ is more effective in preventing the formation of harmful zinc dendrites and accelerates the kinetics of zinc deposition and dissolution compared to $ZnSO_4$.[20] Additionally, $Zn(CF_3SO_3)_2$ broadens the electrochemical window, thus extending the battery range of applications. Previous studies indicate that Zn^{2+} ions form a solvation sheath with water molecules, represented as $(Zn(H_2O)_6)^{2+}$.[9,149] Due to this configuration, a solvated Zn^{2+} ion must overcome a significant energy barrier to desolvate and deposit, which may exacerbate the irreversibility issue for zinc anodes.[9] Additionally, increasing the electrolyte concentration to reduce the number of solvent molecules surrounding the Zn^{2+} ions can modify the solvation structure and the transport dynamics of both cations and anions.[150] This modification can positively impact the zinc stripping/plating process and the overall battery performance. For example, in a Zn/V_2O_5 system, improved electrochemical performance was observed when the concentration of $ZnSO_4$ increased from 0.5 to 3 M.[67] Similarly, Chen et al.[151] demonstrated that in the $Zn/ZnMn_2O_4$ system increasing the concentration of $Zn(CF_3SO_3)_2$ from 1 to 4 M resulted in a Coulombic efficiency of up to 100%. This is partly because a higher electrolyte concentration reduces water activity and water-induced side reactions and mitigates the dissolution of active species such as manganese in the $ZnMn_2O_4$ spinel.

However, higher concentrations also lead to a decreased ionic conductivity and increased solution viscosity. Therefore, selecting an appropriate electrolyte concentration is crucial for optimizing compatibility and performance. As an illustrative case, to further minimize the presence of water molecules surrounding Zn^{2+} ions in the electrolyte, Wang et al.[9] incrementally increased the concentration, ultimately developing a highly concentrated electrolyte consisting of 1 M $Zn(TFSI)_2$ and 20 M LiTFSI, referred to as a "water-in-salt" electrolyte. This approach presents a promising strategy for achieving a highly reversible zinc anode. However, concentrated electrolytes can lead to substantial voltage−polarization even at low current densities (0.2 mA cm^{-2}) and exhibit very low plating/stripping capacities (approximately 0.03 mAh). Additionally, such electrolytes typically result in high viscosity and reduced ionic conductivity, which can adversely affect the rate performance. Furthermore, the higher cost of concentrated electrolytes compared with dilute alternatives may limit their practical, large-scale application.

6. CONCLUSIONS AND OUTLOOK

Various vanadium-based compounds exhibit potential as AZIB cathodes benefiting from the availability of different crystal structures with interesting properties (Figure 10). This review discusses their preparation methods, structural characteristics, electrochemical performance, and ways to enhance the energy storage performance. The present review aims to provide a comprehensive overview of recent advancements in vanadium-based compounds including vanadium oxide and vanadates. It also explores the correlation between structural characteristics and Zn^{2+} storage mechanisms, crucial for developing lightweight materials with high energy content. To expedite high-performance AZIBs, attention is required on the following points:

(i) The phenomenon of capacity fading and cycling stability reduction occurs due to the dissolution of vanadium-based compounds in electrolytes during cycling. Addressing these limitations can be achieved by the modification of electrolytes, the design of integrated electrodes, and the development of cathodes with stable structures.

https://doi.org/10.1021/acsomega.4c06199
ACS Omega 2024, 9, 47920−47938

(ii) The practical applications of vanadium-based compounds are hindered by their inherent low working voltage. Enhancing the voltage window could be achieved by incorporating electron-withdrawing groups into vanadium-based compounds and replacing them with high electronegative atoms or investigating other advanced materials with a wider scope of structural manipulations.

(iii) The cathode material design is significantly influenced by the energy storage mechanism. Numerous energy storage systems have been proposed; however, a consensus has not yet been reached among them. Hence, it is imperative to employ increasingly advanced in situ characterization techniques to provide evidence and pin down the actual storage mechanisms. This is incredibly important to understand the suitability and tune the properties of future modifications in vanadium-based materials to advance their applicability in AZIB cathodes.

(iv) The differential volume changes observed during cycling affect mechanical integrity, and simultaneously intrinsic poor electrical conductivity of vanadium-based materials requires better management. Carbon-based materials, which possess high conductivity, are a viable approach for mitigating this issue. In addition, the enhancement of electrochemical performance in vanadium-based compounds can be achieved through the implementation of metal doping and defect engineering techniques, which effectively alters the chemical environment beneficially.

(v) The multilayer structures of vanadium-based compounds undergo progressive degradation because of the repetitive insertion and extraction of Zn^{2+} ions. Designing and synthesizing core−shell and hollow structures empower the structural stability of vanadium-based compounds.

■ ASSOCIATED CONTENT

Data Availability Statement

No primary research results, software, or code have been included, and no new data were generated or analyzed as part of this review.

■ AUTHOR INFORMATION

Corresponding Author

Bimlesh Lochab − *Materials Chemistry Laboratory, Department of Chemistry, School of Natural Sciences, Shiv Nadar Institution of Eminence, Gautam Buddha Nagar, Uttar Pradesh 201314, India;* orcid.org/0000-0002-8434-6513; Email: bimlesh.lochab@snu.edu.in

Author

Saad Zafar − *Materials Chemistry Laboratory, Department of Chemistry, School of Natural Sciences, Shiv Nadar Institution of Eminence, Gautam Buddha Nagar, Uttar Pradesh 201314, India; Advanced Chemical Energy Research Center, Yokohama National University, 240-8501 Yokohama, Kanagawa, Japan*

Complete contact information is available at: https://pubs.acs.org/10.1021/acsomega.4c06199

Notes

The authors declare no competing financial interest.

■ ACKNOWLEDGMENTS

The authors would like to acknowledge Shiv Nadar Institution of Eminence for the financial support.

■ REFERENCES

(1) Blanc, L. E.; Kundu, D.; Nazar, L. F. Scientific challenges for the implementation of Zn-ion batteries. *Joule* **2020**, *4* (4), 771−799.

(2) Kundu, D.; Adams, B. D.; Duffort, V.; Vajargah, S. H.; Nazar, L. F. A high-capacity and long-life aqueous rechargeable zinc battery using a metal oxide intercalation cathode. *Nat. Energy* **2016**, *1* (10), 1−8.

(3) Tang, B.; Shan, L.; Liang, S.; Zhou, J. Issues and opportunities facing aqueous zinc-ion batteries. *Energy Environ. Sci.* **2019**, *12* (11), 3288−3304.

(4) Pan, H.; Shao, Y.; Yan, P.; Cheng, Y.; Han, K. S.; Nie, Z.; Wang, C.; Yang, J.; Li, X.; Bhattacharya, P.; et al. Reversible aqueous zinc/manganese oxide energy storage from conversion reactions. *Nat. Energy* **2016**, *1* (5), 1−7.

(5) Zhang, N.; Cheng, F.; Liu, J.; Wang, L.; Long, X.; Liu, X.; Li, F.; Chen, J. Rechargeable aqueous zinc-manganese dioxide batteries with high energy and power densities. *Nat. Commun.* **2017**, *8* (1), 1−9.

(6) Chao, D.; Zhou, W.; Ye, C.; Zhang, Q.; Chen, Y.; Gu, L.; Davey, K.; Qiao, S. Z. An electrolytic Zn-MnO_2 battery for high-voltage and scalable energy storage. *Angew. Chem. Int. Ed* **2019**, *131* (23), 7905−7910.

(7) Liu, Y.; Wu, X. Review of vanadium-based electrode materials for rechargeable aqueous zinc ion batteries. *J. Energy Chem.* **2021**, *56*, 223−237.

(8) Linden, D.; Reddy, T. B. *Lithium batteries*; McGraw-Hill: 2002; Vol. 3.

(9) Wang, F.; Borodin, O.; Gao, T.; Fan, X.; Sun, W.; Han, F.; Faraone, A.; Dura, J. A.; Xu, K.; Wang, C. Highly reversible zinc metal anode for aqueous batteries. *Nat. Mater.* **2018**, *17* (6), 543−549.

(10) Xu, C.; Li, B.; Du, H.; Kang, F. Energetic zinc ion chemistry: the rechargeable zinc ion battery. *Angew. Chem., Int. Ed.* **2012**, *51* (4), 933−935.

(11) Xu, X.; Xiong, F.; Meng, J.; Wang, X.; Niu, C.; An, Q.; Mai, L. Vanadium-based nanomaterials: a promising family for emerging metal-ion batteries. *Adv. Funct. Mater.* **2020**, *30* (10), 1904398.

(12) Liu, N.; Li, B.; He, Z.; Dai, L.; Wang, H.; Wang, L. Recent advances and perspectives on vanadium-and manganese-based cathode materials for aqueous zinc ion batteries. *J. Energy Chem.* **2021**, *59*, 134−159.

(13) Guo, C.; Yi, S.; Si, R.; Xi, B.; An, X.; Liu, J.; Li, J.; Xiong, S. Advances on defect engineering of vanadium-based compounds for high-energy aqueous zinc-ion batteries. *Adv. Energy Mater.* **2022**, *12* (40), 2202039.

(14) Zhou, T.; Xiao, H.; Xie, L.; Han, Q.; Qiu, X.; Xiao, Y.; Yang, X.; Zhu, L.; Cao, X. Research on the electrochemical performance of polyoxovanadate material $K_4Na_2V_{10}O_{28}$ as a novel aqueous zinc-ion batteries cathode. *Electrochim. Acta* **2022**, *424*, 140621.

(15) Wang, L.; Zheng, J. Recent advances in cathode materials of rechargeable aqueous zinc-ion batteries. *Mater. Today Adv.* **2020**, *7*, 100078.

(16) Zhang, X.; Yang, W.; Liu, J.; Zhou, Y.; Feng, S.; Yan, S.; Yao, Y.; Wang, G.; Wan, L.; Fang, C.; Zou, Z. Ultralong metahewettite $CaV_6O_{16}\cdot 3H_2O$ nanoribbons as novel host materials for lithium storage: towards high-rate and excellent long-term cyclability. *Nano Energy* **2016**, *22*, 38−47.

(17) Xu, C.; Li, B.; Du, H.; Kang, F. Energetic zinc ion chemistry: the rechargeable zinc ion battery. *Angew. Chem. Int. Ed* **2012**, *51* (4), 933−935.

(18) Alfaruqi, M. H.; Mathew, V.; Gim, J.; Kim, S.; Song, J.; Baboo, J. P.; Choi, S. H.; Kim, J. Electrochemically induced structural transformation in a γ-MnO_2 cathode of a high capacity zinc-ion battery system. *Chem. Mater.* **2015**, *27* (10), 3609−3620.

(19) Sun, W.; Wang, F.; Hou, S.; Yang, C.; Fan, X.; Ma, Z.; Gao, T.; Han, F.; Hu, R.; Zhu, M.; et al. Zn/MnO_2 battery chemistry with H^+ and Zn^{2+} coinsertion. *J. Am. Chem. Soc.* **2017**, *139* (29), 9775−9778.
(20) Wan, F.; Zhang, L.; Dai, X.; Wang, X.; Niu, Z.; Chen, J. Aqueous rechargeable zinc/sodium vanadate batteries with enhanced performance from simultaneous insertion of dual carriers. *Nat. Commun.* **2018**, *9* (1), 1656.
(21) Zhang, L.; Chen, L.; Zhou, X.; Liu, Z. Towards high-voltage aqueous metal-ion batteries beyond 1.5 V: The zinc/zinc hexacyanoferrate system. *Adv. Energy Mater.* **2015**, DOI: 10.1002/aenm.201400930.
(22) Jia, Z.; Wang, B.; Wang, Y. Copper hexacyanoferrate with a well-defined open framework as a positive electrode for aqueous zinc ion batteries. *Mater. Chem. Phys.* **2015**, *149*, 601−606.
(23) Liu, Z.; Pulletikurthi, G.; Endres, F. A prussian blue/zinc secondary battery with a bio-ionic liquid-water mixture as electrolyte. *ACS Appl. Mater. Interfaces* **2016**, *8* (19), 12158−12164.
(24) Trócoli, R.; La Mantia, F. An aqueous zinc-ion battery based on copper hexacyanoferrate. *ChemSusChem* **2015**, *8* (3), 481−485.
(25) Chae, M. S.; Heo, J. W.; Kwak, H. H.; Lee, H.; Hong, S.-T. Organic electrolyte-based rechargeable zinc-ion batteries using potassium nickel hexacyanoferrate as a cathode material. *J. Power Sources* **2017**, *337*, 204−211.
(26) Gupta, T.; Kim, A.; Phadke, S.; Biswas, S.; Luong, T.; Hertzberg, B. J.; Chamoun, M.; Evans-Lutterodt, K.; Steingart, D. A. Improving the cycle life of a high-rate, high-potential aqueous dual-ion battery using hyper-dendritic zinc and copper hexacyanoferrate. *J. Power Sources* **2016**, *305*, 22−29.
(27) Li, G.; Yang, Z.; Jiang, Y.; Jin, C.; Huang, W.; Ding, X.; Huang, Y. Towards polyvalent ion batteries: A zinc-ion battery based on NASICON structured Na3V2 (PO4) 3. *Nano Energy* **2016**, *25*, 211−217.
(28) Li, G.; Yang, Z.; Jiang, Y.; Zhang, W.; Huang, Y. Hybrid aqueous battery based on Na3V2 (PO4) 3/C cathode and zinc anode for potential large-scale energy storage. *J. Power Sources* **2016**, *308*, 52−57.
(29) Zhao, H.; Hu, C.; Cheng, H.; Fang, J.; Xie, Y.; Fang, W.; Doan, T.; Hoang, T.; Xu, J.; Chen, P. Novel rechargeable $M_3V_2(PO_4)_3$// zinc (M= Li, Na) hybrid aqueous batteries with excellent cycling performance. *Sci. Rep.* **2016**, *6* (1), 25809.
(30) Zhao, J.; Li, Y.; Peng, X.; Dong, S.; Ma, J.; Cui, G.; Chen, L. High-voltage Zn/$LiMn_{0.8}Fe_{0.2}PO_4$ aqueous rechargeable battery by virtue of "water-in-salt" electrolyte. *Electrochem. commun.* **2016**, *69*, 6−10.
(31) Wan, F.; Zhang, L.; Dai, X.; Wang, X.; Niu, Z.; Chen, J. Aqueous rechargeable zinc/sodium vanadate batteries with enhanced performance from simultaneous insertion of dual carriers. *Nat. Commun.* **2018**, *9* (1), 1656.
(32) Lai, J.; Zhu, H.; Zhu, X.; Koritala, H.; Wang, Y. Interlayer-expanded $V_6O_{13}\cdot nH_2O$ architecture constructed for an advanced rechargeable aqueous zinc-ion battery. *ACS Appl. Energy Mater.* **2019**, *2* (3), 1988−1996.
(33) Huang, J.; Zeng, J.; Zhu, K.; Zhang, R.; Liu, J. High-Performance Aqueous Zinc-Manganese Battery with Reversible Mn^{2+}/Mn^{4+} Double Redox Achieved by Carbon Coated MnO_x Nanoparticles. *Nano-Micro Lett.* **2020**, *12*, 1−12.
(34) Lu, Y.; Zhu, T.; van den Bergh, W.; Stefik, M.; Huang, K. A high performing Zn-ion battery cathode enabled by in situ transformation of V_2O_5 atomic layers. *Angew. Chem., Int. Ed.* **2020**, *132* (39), 17152−17159.
(35) Wang, X.; Zhang, Z.; Huang, M.; Feng, J.; Xiong, S.; Xi, B. In situ electrochemically activated vanadium oxide cathode for advanced aqueous Zn-ion batteries. *Nano Lett.* **2022**, *22* (1), 119−127.
(36) Xu, X.; Xiong, F.; Meng, J.; Wang, X.; Niu, C.; An, Q.; Mai, L. Vanadium-Based Nanomaterials: A Promising Family for Emerging Metal-Ion Batteries. *Adv. Funct. Mater.* **2020**, *30* (10), 1904398.
(37) Xu, W.; Liu, C.; Wu, Q.; Xie, W.; Kim, W.-Y.; Lee, S.-Y.; Gwon, J. A stretchable solid-state zinc ion battery based on a cellulose nanofiber-polyacrylamide hydrogel electrolyte and a $Mg_{0.23}V_2O_5\cdot 1.0H_2O$ cathode. *J. Mater. Chem. A* **2020**, *8* (35), 18327−18337.
(38) Islam, S.; Alfaruqi, M. H.; Sambandam, B.; Putro, D. Y.; Kim, S.; Jo, J.; Kim, S.; Mathew, V.; Kim, J. A new rechargeable battery based on a zinc anode and a NaV6O15 nanorod cathode. *Chem. Commun.* **2019**, *55* (26), 3793−3796.
(39) Song, M.; Tan, H.; Chao, D.; Fan, H. J. Recent advances in Zn-ion batteries. *Adv. Funct. Mater.* **2018**, *28* (41), 1802564.
(40) Zavalij, P. Y.; Whittingham, M. S. Structural chemistry of vanadium oxides with open frameworks. *Acta Crystallographica Section B* **1999**, *55* (5), 627−663.
(41) Wu, Y.; Song, T.-Y.; Chen, L.-N. A review on recent developments of vanadium-based cathode for rechargeable zinc-ion batteries. *Tungsten* **2021**, *3* (3), 289−304.
(42) Zhang, Y.; Ang, E. H.; Dinh, K. N.; Rui, K.; Lin, H.; Zhu, J.; Yan, Q. Recent advances in vanadium-based cathode materials for rechargeable zinc ion batteries. *Mater. Chem. Front.* **2021**, *5* (2), 744−762.
(43) Zhou, Y.; Chen, F.; Arandiyan, H.; Guan, P.; Liu, Y.; Wang, Y.; Zhao, C.; Wang, D.; Chu, D. Oxide-based cathode materials for rechargeable zinc ion batteries: Progresses and challenges. *J. Energy Chem.* **2021**, *57*, 516−542.
(44) Lee, S.; Hippalgaonkar, K.; Yang, F.; Hong, J.; Ko, C.; Suh, J.; Liu, K.; Wang, K.; Urban, J. J.; Zhang, X.; Dames, C.; Hartnoll, S. A.; Delaire, O.; Wu, J. Anomalously low electronic thermal conductivity in metallic vanadium dioxide. *Science* **2017**, *355* (6323), 371−374.
(45) Lee, S.; Ivanov, I. N.; Keum, J. K.; Lee, H. N. Epitaxial stabilization and phase instability of VO2 polymorphs. *Sci. Rep.* **2016**, *6*, 19621.
(46) Park, J.-S.; Jo, J. H.; Aniskevich, Y.; Bakavets, A.; Ragoisha, G.; Streltsov, E.; Kim, J.; Myung, S.-T. Open-structured vanadium dioxide as an intercalation host for Zn ions: Investigation by first-principles calculation and experiments. *Chem. Mater.* **2018**, *30* (19), 6777−6787.
(47) Chen, L.; Ruan, Y.; Zhang, G.; Wei, Q.; Jiang, Y.; Xiong, T.; He, P.; Yang, W.; Yan, M.; An, Q.; Mai, L. Ultrastable and high-performance Zn/VO_2 battery based on a reversible single-phase reaction. *Chem. Mater.* **2019**, *31* (3), 699−706.
(48) Li, Z.; Ren, Y.; Mo, L.; Liu, C.; Hsu, K.; Ding, Y.; Zhang, X.; Li, X.; Hu, L.; Ji, D.; Cao, G. Impacts of Oxygen Vacancies on Zinc Ion Intercalation in VO2. *ACS Nano* **2020**, *14* (5), 5581−5589.
(49) Ding, J.; Du, Z.; Gu, L.; Li, B.; Wang, L.; Wang, S.; Gong, Y.; Yang, S. Ultrafast Zn^{2+} intercalation and deintercalation in vanadium dioxide. *Adv. Mater.* **2018**, *30* (26), 1800762.
(50) Deng, S.; Li, H.; Chen, B.; Xu, Z.; Jiang, Y.; Li, C.; Xiao, W.; Yan, X. High performance of Mn-doped VO2 cathode for aqueous zinc-ion batteries: an insight into Zn2+ storage mechanism. *Chem. Eng. J.* **2023**, *452*, 139115.
(51) Cai, Y.; Chua, R.; Kou, Z.; Ren, H.; Yuan, D.; Huang, S.; Kumar, S.; Verma, V.; Amonpattaratkit, P.; Srinivasan, M. Boosting Zn-ion storage performance of bronze-type VO2 via Ni-mediated electronic structure engineering. *ACS Appl. Mater. Interfaces* **2020**, *12* (32), 36110−36118.
(52) Wang, S.; Zhang, H.; Zhao, K.; Liu, W.; Luo, N.; Zhao, J.; Wu, S.; Ding, J.; Fang, S.; Cheng, F. Designing interstitial boron-doped tunnel-type vanadium dioxide cathode for enhancing zinc ion storage capability. *Carbon Energy* **2023**, *5* (8), No. e330.
(53) He, Q.; Hu, T.; Wu, Q.; Wang, C.; Han, X.; Chen, Z.; Zhu, Y.; Chen, J.; Zhang, Y.; Shi, L.; Wang, X.; Ma, Y.; Zhao, J. Tunnel-Oriented VO_2 (B) cathode for high-rate aqueous zinc-ion batteries. *Adv. Mater.* **2024**, 2400888.
(54) Jiang, L.; Qu, Y.; Ren, Z.; Yu, P.; Zhao, D.; Zhou, W.; Wang, L.; Fu, H. In situ carbon-coated yolk-shell V_2O_3 microspheres forl lithium ion batteries. *ACS Appl. Mater. Interfaces* **2015**, *7* (3), 1595−1601.
(55) Jin, T.; Li, H.; Li, Y.; Jiao, L.; Chen, J. Intercalation pseudocapacitance in flexible and self-standing V2O3 porous nanofibers for high-rate and ultra-stable K ion storage. *Nano Energy* **2018**, *50*, 462−467.

https://doi.org/10.1021/acsomega.4c06199
ACS Omega 2024, 9, 47920−47938

(56) Yi, T.-F.; Qiu, L.; Qu, J.-P.; Liu, H.; Zhang, J.-H.; Zhu, Y.-R. Towards high-performance cathodes: Design and energy storage mechanism of vanadium oxides-based materials for aqueous Zn-ion batteries. *Coord. Chem. Rev.* **2021**, *446*, 214124.
(57) Ding, Y.; Peng, Y.; Chen, S.; Zhang, X.; Li, Z.; Zhu, L.; Mo, L.-E.; Hu, L. Hierarchical porous metallic V_2O_3@C for advanced aqueous zinc-ion batteries. *ACS Appl. Mater. Interfaces* **2019**, *11* (47), 44109−44117.
(58) Ding, J.; Zheng, H.; Gao, H.; Liu, Q.; Hu, Z.; Han, L.; Wang, S.; Wu, S.; Fang, S.; Chou, S. In situ lattice tunnel distortion of vanadium trioxide for enhancing zinc ion storage. *Adv. Energy Mater.* **2021**, *11* (26), 2100973.
(59) Wu, J.; Liang, H.; Li, J.; Yang, Z.; Cai, J. Facile preparation of urchin-like morphology V_2O_3-VN nano-heterojunction cathodes for high-performance aqueous zinc ion battery. *J. Colloid Interface Sci.* **2024**, *654*, 46−55.
(60) Chen, X.; Kong, Q.; Wu, X.; An, X.; Zhang, J.; Wang, Q.; Yao, W. V_2O_3@C optimized by carbon regulation strategy for ultra long-life aqueous zinc-ion batteries. *Chem. Eng. J.* **2023**, *451*, 138765.
(61) Wang, D.; Liang, W.; He, X.; Yang, Y.; Wang, S.; Li, J.; Wang, J.; Jin, H. V_2O_3@C microspheres as the high-performance cathode materials for advanced aqueous zinc-ion storage. *ACS Appl. Mater. Interfaces* **2023**, *15* (17), 20876−20884.
(62) Chen, R.; Luo, R.; Huang, Y.; Wu, F.; Li, L. Advanced high energy density secondary batteries with multi-electron reaction materials. *Adv. Sci.* **2016**, *3* (10), 1600051.
(63) Javed, M. S.; Shah, S. S. A.; Najam, T.; Siyal, S. H.; Hussain, S.; Saleem, M.; Zhao, Z.; Mai, W. Achieving high-energy density and superior cyclic stability in flexible and lightweight pseudocapacitor through synergic effects of binder-free $CoGa_2O_4$ 2D-hexagonal nanoplates. *Nano Energy* **2020**, *77*, 105276.
(64) Chen, D.; Rui, X.; Zhang, Q.; Geng, H.; Gan, L.; Zhang, W.; Li, C.; Huang, S.; Yu, Y. Persistent zinc-ion storage in mass-produced V_2O_5 architectures. *Nano Energy* **2019**, *60*, 171−178.
(65) Zhang, N.; Dong, Y.; Jia, M.; Bian, X.; Wang, Y.; Qiu, M.; Xu, J.; Liu, Y.; Jiao, L.; Cheng, F. Rechargeable aqueous Zn-V_2O_5 battery with high eergy density and long cycle life. *ACS Energy Lett.* **2018**, *3* (6), 1366−1372.
(66) Zhang, L.; Chen, L.; Zhou, X.; Liu, Z. Towards high-voltage aqueous metal-ion batteries beyond 1.5 V: The zinc/zinc hexacyanoferrate system. *Adv. Energy Mater.* **2015**, *5* (2), 1400930.
(67) Zhou, J.; Shan, L.; Wu, Z.; Guo, X.; Fang, G.; Liang, S. Investigation of V_2O_5 as a low-cost rechargeable aqueous zinc ion battery cathode. *Chem. Commun.* **2018**, *54* (35), 4457−4460.
(68) Li, Y.; Huang, Z.; Kalambate, P. K.; Zhong, Y.; Huang, Z.; Xie, M.; Shen, Y.; Huang, Y. V_2O_5 nanopaper as a cathode material with high capacity and long cycle life for rechargeable aqueous zinc-ion battery. *Nano Energy* **2019**, *60*, 752−759.
(69) Chen, X.; Wang, L.; Li, H.; Cheng, F.; Chen, J. Porous V_2O_5 nanofibers as cathode materials for rechargeable aqueous zinc-ion batteries. *J. Energy Chem.* **2019**, *38*, 20−25.
(70) Javed, M. S.; Lei, H.; Wang, Z.; Liu, B.-t.; Cai, X.; Mai, W. 2D V_2O_5 nanosheets as a binder-free high-energy cathode for ultrafast aqueous and flexible Zn-ion batteries. *Nano Energy* **2020**, *70*, 104573.
(71) Liu, F.; Chen, Z.; Fang, G.; Wang, Z.; Cai, Y.; Tang, B.; Zhou, J.; Liang, S. V_2O_5 nanospheres with mixed vanadium valences as high electrochemically active aqueous zinc-ion battery cathode. *Nano-Micro Lett.* **2019**, *11* (1), 25.
(72) Fan, L.; Ru, Y.; Xue, H.; Pang, H.; Xu, Q. Vanadium-based materials as positive electrode for aqueous zinc-ion batteries. *Adv. Sustain. Syst.* **2020**, *4* (12), 2000178.
(73) Zhang, N.; Dong, Y.; Jia, M.; Bian, X.; Wang, Y.; Qiu, M.; Xu, J.; Liu, Y.; Jiao, L.; Cheng, F. Rechargeable aqueous Zn-V_2O_5 battery with high energy density and long cycle life. *ACS Energy Lett.* **2018**, *3* (6), 1366−1372.
(74) Linghu, S.; Ye, J.; Deng, K.; Liu, P.; Zhong, Y.; You, T.; Tian, W.; Ji, J. Coupling of V_2O_5 structural design and electrolyte modulation toward stable zinc-ion battery. *J. Power Sources* **2024**, *592*, 233922.
(75) Zafar, S.; Sharma, M.; Shai Mp, K.; Karmodak, N.; Singh, S. K.; Lochab, B. A layer separated V_2O_5-PEG-amine hybrid cathode material for high capacity zinc-ion batteries. *J. Mater. Chem. A* **2024**, DOI: 10.1039/D4TA01656D.
(76) Li, J.; Guo, P.; Chen, G.; Wu, C.; Xiao, Y.; Dong, H.; Liang, Y.; Liu, Y.; Hu, H.; Zheng, M. Chitosan-derived carbon dots introduced V_2O_5 nanobelts for high-performance aqueous zinc-ion battery. *J. Energy Storage* **2024**, *84*, 110632.
(77) Jia, D.; Shen, Z.; Lv, Y.; Chen, Z.; Li, H.; Yu, Y.; Qiu, J.; He, X. In situ electrochemical tuning of MIL-88B(V)@rGO into amorphous V_2O_5@rGO as cathode for high-performance aqueous zinc-ion battery. *Adv. Funct. Mater.* **2024**, *34* (2), 2308319.
(78) Clites, M.; Hart, J. L.; Taheri, M. L.; Pomerantseva, E. Chemically preintercalated bilayered $K_xV_2O_5{\cdot}nH_2O$ nanobelts as a high-performing cathode material for K-ion batteries. *ACS Energy Lett.* **2018**, *3* (3), 562−567.
(79) Yang, Y.; Tang, Y.; Liang, S.; Wu, Z.; Fang, G.; Cao, X.; Wang, C.; Lin, T.; Pan, A.; Zhou, J. Transition metal ion-preintercalated V_2O_5 as high-performance aqueous zinc-ion battery cathode with broad temperature adaptability. *Nano Energy* **2019**, *61*, 617−625.
(80) Alfaruqi, M. H.; Mathew, V.; Song, J.; Kim, S.; Islam, S.; Pham, D. T.; Jo, J.; Kim, S.; Baboo, J. P.; Xiu, Z.; Lee, K.-S.; Sun, Y.-K.; Kim, J. Electrochemical zinc intercalation in lithium vanadium oxide: A high-capacity zinc-ion battery cathode. *Chem. Mater.* **2017**, *29* (4), 1684−1694.
(81) He, P.; Yan, M.; Liao, X.; Luo, Y.; Mai, L.; Nan, C.-W. Reversible V^{3+}/V^{5+} double redox in lithium vanadium oxide cathode for zinc storage. *Energy Storage Mater.* **2020**, *29*, 113−120.
(82) Guo, X.; Fang, G.; Zhang, W.; Zhou, J.; Shan, L.; Wang, L.; Wang, C.; Lin, T.; Tang, Y.; Liang, S. Mechanistic insights of Zn^{2+} storage in sodium vanadates. *Adv. Energy Mater.* **2018**, *8* (27), 1801819.
(83) He, P.; Zhang, G.; Liao, X.; Yan, M.; Xu, X.; An, Q.; Liu, J.; Mai, L. Sodium ion stabilized vanadium oxide nanowire cathode for high-performance zinc-ion batteries. *Adv. Energy Mater.* **2018**, *8* (10), 1702463.
(84) Tang, B.; Fang, G.; Zhou, J.; Wang, L.; Lei, Y.; Wang, C.; Lin, T.; Tang, Y.; Liang, S. Potassium vanadates with stable structure and fast ion diffusion channel as cathode for rechargeable aqueous zinc-ion batteries. *Nano Energy* **2018**, *51*, 579−587.
(85) Sambandam, B.; Soundharrajan, V.; Kim, S.; Alfaruqi, M. H.; Jo, J.; Kim, S.; Mathew, V.; Sun, Y.-k.; Kim, J. Aqueous rechargeable Zn-ion batteries: an imperishable and high-energy $Zn_2V_2O_7$ nanowire cathode through intercalation regulation. *J. Mater. Chem. A* **2018**, *6* (9), 3850−3856.
(86) Zhou, F.; Lin, Y.; Li, T.; Zhang, S.; Deng, C. Forming bubble-encapsulated double-shelled hollow spheres towards fast kinetics and superior high rate performance for aqueous rechargeable Zn-ion batteries. *J. Mater. Chem. A* **2019**, *7* (17), 10589−10600.
(87) Xia, C.; Guo, J.; Li, P.; Zhang, X.; Alshareef, H. N. Highly stable aqueous zinc-Ion storage using a layered calcium vanadium oxide bronze cathode. *Angew. Chem., Int. Ed.* **2018**, *57* (15), 3943−3948.
(88) Zhang, Y.; Wan, F.; Huang, S.; Wang, S.; Niu, Z.; Chen, J. A chemically self-charging aqueous zinc-ion battery. *Nat. Commun.* **2020**, *11* (1), 2199.
(89) Ming, F.; Liang, H.; Lei, Y.; Kandambeth, S.; Eddaoudi, M.; Alshareef, H. N. Layered $Mg_xV_2O_5{\cdot}nH_2O$ as cathode material for high-performance aqueous zinc ion batteries. *ACS Energy Lett.* **2018**, *3* (10), 2602−2609.
(90) Zhou, W.; Chen, J.; Chen, M.; Wang, A.; Huang, A.; Xu, X.; Xu, J.; Wong, C.-P. An environmentally adaptive quasi-solid-state zinc-ion battery based on magnesium vanadate hydrate with commercial-level mass loading and anti-freezing gel electrolyte. *J. Mater. Chem. A* **2020**, *8* (17), 8397−8409.
(91) Guan, J.; Shao, L.; Yu, L.; Wang, S.; Shi, X.; Cai, J.; Sun, Z. Two-dimensional $Mg_{0.2}V_2O_5{\cdot}nH_2O$ nanobelts derived from V_4C_3 MXenes for highly stable aqueous zinc ion batteries. *Chem. Eng.* **2022**, *443*, 136502.

(92) Du, Y.-H.; Liu, X.-Y.; Wang, X.-Y.; Sun, J.-C.; Lu, Q.-Q.; Wang, J.-Z.; Omar, A.; Mikhailova, D. Freestanding strontium vanadate/carbon nanotube films for long-life aqueous zinc-ion batteries. *Rare Met.* **2022**, *41* (2), 415−424.
(93) Guo, J.; Ming, J.; Lei, Y.; Zhang, W.; Xia, C.; Cui, Y.; Alshareef, H. N. Artificial solid electrolyte interphase for suppressing surface reactions and cathode dissolution in aqueous zinc ion batteries. *ACS Energy Lett.* **2019**, *4* (12), 2776−2781.
(94) Wan, F.; Niu, Z. Design strategies for vanadium-based aqueous zinc-ion batteries. *Angew. Chem. Int. Ed.* **2019**, *58* (46), 16358−16367.
(95) Wang, X.; Xi, B.; Ma, X.; Feng, Z.; Jia, Y.; Feng, J.; Qian, Y.; Xiong, S. Boosting zinc-ion storage capability by effectively suppressing vanadium dissolution based on robust layered barium vanadate. *Nano Lett.* **2020**, *20* (4), 2899−2906.
(96) Shan, L.; Zhou, J.; Han, M.; Fang, G.; Cao, X.; Wu, X.; Liang, S. Reversible Zn-driven reduction displacement reaction in aqueous zinc-ion battery. *J. Mater. Chem. A* **2019**, *7* (13), 7355−7359.
(97) Wang, H.; Huang, K.; Huang, C.; Liu, S.; Ren, Y.; Huang, X. $(NH_4)_{0.5}V_2O_5$ nanobelt with good cycling stability as cathode material for Li-ion battery. *J. Power Sources* **2011**, *196* (13), 5645−5650.
(98) Li, Q.; Rui, X.; Chen, D.; Feng, Y.; Xiao, N.; Gan, L.; Zhang, Q.; Yu, Y.; Huang, S. A high-capacity ammonium vanadate cathode for zinc-ion battery. *Nano-Micro Lett.* **2020**, *12* (1), 67.
(99) Jiang, H.; Zhang, Y.; Liu, Y.; Yang, J.; Xu, L.; Wang, P.; Gao, Z.; Zheng, J.; Meng, C.; Pan, Z. In situ grown 2D hydrated ammonium vanadate nanosheets on carbon cloth as a free-standing cathode for high-performance rechargeable Zn-ion batteries. *J. Mater. Chem. A* **2020**, *8* (30), 15130−15139.
(100) Jiang, Y.; Wu, Z.; Ye, F.; Pang, R.; Zhang, L.; Liu, Q.; Chang, X.; Sun, S.; Sun, Z.; Hu, L. Spontaneous knitting behavior of 6.7-nm thin $(NH_4)_{0.38}V_2O_5$ nano- ribbons for binder-free zinc-ion batteries. *Energy Storage Mater.* **2021**, *42*, 286−294.
(101) Xia, C.; Guo, J.; Lei, Y.; Liang, H.; Zhao, C.; Alshareef, H. N. Rechargeable aqueous zinc-ion battery based on porous framework zinc pyrovanadate intercalation cathode. *Adv. Mater.* **2018**, *30* (5), 1705580.
(102) Tang, B.; Zhou, J.; Fang, G.; Liu, F.; Zhu, C.; Wang, C.; Pan, A.; Liang, S. Engineering the interplanar spacing of ammonium vanadates as a high-performance aqueous zinc-ion battery cathode. *J. Mater. Chem. A* **2019**, *7* (3), 940−945.
(103) Soundharrajan, V.; Sambandam, B.; Kim, S.; Alfaruqi, M. H.; Putro, D. Y.; Jo, J.; Kim, S.; Mathew, V.; Sun, Y.-K.; Kim, J. $Na_2V_6O_{16}\cdot 3H_2O$ barnesite nanorod: An open door to display a stable and high energy for aqueous rechargeable Zn-ion batteries as cathodes. *Nano Lett.* **2018**, *18* (4), 2402−2410.
(104) Wei, T.; Li, Q.; Yang, G.; Wang, C. Highly reversible and long-life cycling aqueous zinc-ion battery based on ultrathin $(NH_4)_2V_{10}O_{25}\cdot 8H_2O$ nanobelts. *J. Mater. Chem. A* **2018**, *6* (41), 20402−20410.
(105) Trócoli, R.; La Mantia, F. An Aqueous Zinc-Ion Battery Based on Copper Hexacyanoferrate. *ChemSusChem* **2015**, *8* (3), 481−485.
(106) Chen, S.; Zhang, Y.; Geng, H.; Yang, Y.; Rui, X.; Li, C. C. Zinc ions pillared vanadate cathodes by chemical pre-intercalation towards long cycling life and low-temperature zinc ion batteries. *J. Power Sources* **2019**, *441*, 227192.
(107) Wang, X.; Xi, B.; Feng, Z.; Chen, W.; Li, H.; Jia, Y.; Feng, J.; Qian, Y.; Xiong, S. Layered $(NH_4)_2V_6O_{16}\cdot 1.5H_2O$ nanobelts as a high-performance cathode for aqueous zinc-ion batteries. *J. Mater. Chem. A* **2019**, *7* (32), 19130−19139.
(108) Kim, H.; Lim, H.; Kim, H.-S.; Kim, K. J.; Byun, D.; Choi, W. Polydopamine-derived N-doped carbon-wrapped $Na_3V_2(PO_4)_3$ cathode with superior rate capability and cycling stability for sodium-ion batteries. *Nano Res.* **2019**, *12* (2), 397−404.
(109) Li, H.; Xu, M.; Zhang, Z.; Lai, Y.; Ma, J. Engineering of polyanion type cathode materials for sodium-ion batteries: Toward higher energy/power density. *Adv. Funct. Mater.* **2020**, *30* (28), 2000473.
(110) Fang, Y.; Xiao, L.; Ai, X.; Cao, Y.; Yang, H. Hierarchical carbon framework wrapped $Na_3V_2(PO_4)_3$ as a superior high-rate and extended lifespan cathode for sodium-ion batteries. *Adv. Mater.* **2015**, *27* (39), 5895−5900.
(111) Li, G.; Yang, Z.; Jiang, Y.; Jin, C.; Huang, W.; Ding, X.; Huang, Y. Towards polyvalent ion batteries: A zinc-ion battery based on NASICON structured $Na_3V_2(PO_4)_3$. *Nano Energy* **2016**, *25*, 211−217.
(112) Li, W.; Wang, K.; Cheng, S.; Jiang, K. A long-life aqueous Zn-ion battery based on $Na_3V_2(PO_4)_2F_3$ cathode. *Energy Storage Mater.* **2018**, *15*, 14−21.
(113) Guan, J.; Huang, Q.; Shao, L.; Shi, X.; Zhao, D.; Wang, L.; Sun, Z. Polyanion-type $Na_3V_2(PO_4)_2F_3$@rGO with high-voltage and ultralong-life for aqueous zinc ion batteries. *Small* **2023**, *19* (15), 2207148.
(114) Wang, F.; Sun, W.; Shadike, Z.; Hu, E.; Ji, X.; Gao, T.; Yang, X.-Q.; Xu, K.; Wang, C. How water accelerates bivalent Ion diffusion at the electrolyte/electrode interface. *Angew. Chem., Int. Ed.* **2018**, *57* (37), 11978−11981.
(115) Zhao, D.; Pu, X.; Wang, C.; Pan, Z.; Ding, M.; Cao, Y.; Chen, Z. Low-strain layered $Zn_{0.56}VOPO_4\bullet 2H_2O$ as a high-voltage and long-lifespan cathode material for Zn-ion batteries. *Energy Storage Mater.* **2024**, *66*, 103239.
(116) Tan, C.; Zhang, H. Two-dimensional transition metal dichalcogenide nanosheet-based composites. *Chem. Soc. Rev.* **2015**, *44* (9), 2713−2731.
(117) Wu, L.; Sun, R.; Xiong, F.; Pei, C.; Han, K.; Peng, C.; Fan, Y.; Yang, W.; An, Q.; Mai, L. A rechargeable aluminum-ion battery based on a VS_2 nanosheet cathode. *Phys. Chem. Chem. Phys.* **2018**, *20* (35), 22563−22568.
(118) He, P.; Yan, M.; Zhang, G.; Sun, R.; Chen, L.; An, Q.; Mai, L. Layered VS_2 nanosheet-based aqueous Zn ion battery cathode. *Adv. Energy Mater.* **2017**, *7* (11), 1601920.
(119) Zafar, S.; Singh, S. K.; Lochab, B. Nano-wired polyaniline/VS_2 composite materials for quasi-solid-state supercapacitor and zinc-ion battery applications. *Mater. Adv.* **2023**, *4* (11), 2425−2436.
(120) Britto, S.; Leskes, M.; Hua, X.; Hébert, C.-A.; Shin, H. S.; Clarke, S.; Borkiewicz, O.; Chapman, K. W.; Seshadri, R.; Cho, J.; Grey, C. P. Multiple redox modes in the reversible lithiation of high-capacity, peierls-distorted vanadium sulfide. *J. Am. Chem. Soc.* **2015**, *137* (26), 8499−8508.
(121) Zhou, Y.; Li, Y.; Yang, J.; Tian, J.; Xu, H.; Yang, J.; Fan, W. Conductive polymer-coated VS_4 submicrospheres as advanced electrode materials in lithium-ion batteries. *ACS Appl. Mater. Interfaces* **2016**, *8* (29), 18797−18805.
(122) Zafar, S.; Thomas, A.; Mahapatra, S. N.; Karmodak, N.; Arora, H. S.; Lochab, B. Morphology-dependent enhancement of the electrochemical performance of CNF-guided tunable VS_4 heterostructures for symmetric supercapacitors. *J. Mater. Chem. A* **2023**, *11* (39), 21263−21271.
(123) Qin, H.; Yang, Z.; Chen, L.; Chen, X.; Wang, L. A high-rate aqueous rechargeable zinc ion battery based on the VS_4@rGO nanocomposite. *J. Mater. Chem. A* **2018**, *6* (46), 23757−23765.
(124) Rong, Y.; Chen, H.; Wu, J.; Yang, Z.; Deng, L.; Fu, Z. Granular vanadium nitride (VN) cathode for high-capacity and stable zinc-ion batteries. *Ind. Eng. Chem. Res.* **2021**, *60* (24), 8649−8658.
(125) Yao, X.; Khanam, Z.; Li, C.; Koroma, M.; Ouyang, T.; Hu, Y. w.; Shen, K.; Balogun, M. S. Unlatching the additional zinc storage ability of vanadium nitride nanocrystallites. *Small* **2024**, *20*, 2312036.
(126) Deng, L.; Chen, H.; Wu, J.; Yang, Z.; Rong, Y.; Fu, Z. V_2O_3 as cathode of zinc ion battery with high stability and long cycling life. *Ionics* **2021**, *27* (8), 3393−3402.
(127) Wu, S.; Ding, Y.; Hu, L.; Zhang, X.; Huang, Y.; Chen, S. Amorphous V_2O_5 as high performance cathode for aqueous zinc ion battery. *Mater. Lett.* **2020**, *277*, 128268.
(128) Li, R.; Zhang, H.; Zheng, Q.; Li, X. Porous V_2O_5 yolk-shell microspheres for zinc ion battery cathodes: activation responsible for enhanced capacity and rate performance. *J. Mater. Chem. A* **2020**, *8* (10), 5186−5193.

https://doi.org/10.1021/acsomega.4c06199
ACS Omega 2024, 9, 47920−47938

(129) Yin, B.; Zhang, S.; Ke, K.; Xiong, T.; Wang, Y.; Lim, B. K. D.; Lee, W. S. V.; Wang, Z.; Xue, J. Binder-free V_2O_5/CNT paper electrode for high rate performance zinc ion battery. *Nanoscale* **2019**, *11* (42), 19723−19728.
(130) Liu, C.; Li, R.; Liu, W.; Shen, G.; Chen, D. Chitosan-assisted fabrication of a network C@V_2O_5 cathode for high-performance Zn-ion batteries. *ACS Appl. Mater. Interfaces* **2021**, *13* (31), 37194−37200.
(131) Wei, T.; Li, Q.; Yang, G.; Wang, C. An electrochemically induced bilayered structure facilitates long-life zinc storage of vanadium dioxide. *J. Mater. Chem. A* **2018**, *6* (17), 8006−8012.
(132) Cai, Y.; Liu, F.; Luo, Z.; Fang, G.; Zhou, J.; Pan, A.; Liang, S. Pilotaxitic $Na_{1.1}V_3O_{7.9}$ nanoribbons/graphene as high-performance sodium ion battery and aqueous zinc ion battery cathode. *Energy Storage Mater.* **2018**, *13*, 168−174.
(133) Yang, Y.; Tang, Y.; Fang, G.; Shan, L.; Guo, J.; Zhang, W.; Wang, C.; Wang, L.; Zhou, J.; Liang, S. Li^+ intercalated $V_2O_5{\cdot}nH_2O$ with enlarged layer spacing and fast ion diffusion as an aqueous zinc-ion battery cathode. *Energy Environ. Sci.* **2018**, *11* (11), 3157−3162.
(134) Zhu, K.; Wu, T.; Huang, K. A high capacity bilayer cathode for aqueous Zn-ion batteries. *ACS Nano* **2019**, *13* (12), 14447−14458.
(135) Li, Q.; Liu, Y.; Ma, K.; Yang, G.; Wang, C. In situ Ag nanoparticles reinforced pseudo-Zn-Air reaction boosting $Ag_2V_4O_{11}$ as high-performance cathode material for aqueous zinc-ion batteries. *Small Methods* **2019**, *3* (12), 1900637.
(136) Hao, Y.; Zhang, S.; Tao, P.; Shen, T.; Huang, Z.; Yan, J.; Chen, Y. Pillaring effect of K ion anchoring for stable V_2O_5-based zinc-ion battery cathodes. *ChemNanoMat* **2020**, *6* (5), 797−805.
(137) Yu, X.; Hu, F.; Cui, F.; Zhao, J.; Guan, C.; Zhu, K. The displacement reaction mechanism of the CuV_2O_6 nanowire cathode for rechargeable aqueous zinc ion batteries. *Dalton Trans.* **2020**, *49* (4), 1048−1055.
(138) Hu, T.; Feng, Z.; Zhang, Y.; Liu, Y.; Sun, J.; Zheng, J.; Jiang, H.; Wang, P.; Dong, X.; Meng, C. Double guarantee mechanism" of Ca^{2+}-intercalation and rGO-integration ensures hydrated vanadium oxide with high performance for aqueous zinc-ion batteries. *Inorg. Chem. Front.* **2021**, *8* (1), 79−89.
(139) Wu, J.; Kuang, Q.; Zhang, K.; Feng, J.; Huang, C.; Li, J.; Fan, Q.; Dong, Y.; Zhao, Y. Spinel $Zn_3V_3O_8$: A high-capacity zinc supplied cathode for aqueous Zn-ion batteries. *Energy Storage Mater.* **2021**, *41*, 297−309.
(140) Luo, C.; Xiao, L.; Wu, X. Aqueous zinc ion batteries based on sodium vanadate electrode materials with long lifespan and high energy density. *Mater. Adv.* **2022**, *3* (1), 604−610.
(141) Zhu, K.; Wu, T.; van den Bergh, W.; Stefik, M.; Huang, K. Reversible molecular and ionic storage mechanisms in high-performance $Zn_{0.1}V_2O_5{\cdot}nH_2O$ xerogel cathode for aqueous Zn-ion batteries. *ACS Nano* **2021**, *15* (6), 10678−10688.
(142) Bin, D.; Liu, Y.; Yang, B.; Huang, J.; Dong, X.; Zhang, X.; Wang, Y.; Xia, Y. Engineering a high-energy-density and long Lifespan aqueous zinc battery via ammonium vanadium bronze. *ACS Appl. Mater. Interfaces* **2019**, *11* (23), 20796−20803.
(143) Li, W.; Wang, K.; Cheng, S.; Jiang, K. A long-life aqueous Zn-ion battery based on $Na_3V_2(PO_4)_2F_3$ cathode. *Energy Storage Mater.* **2018**, *15*, 14−21.
(144) Li, M.; Li, Z.; Wang, X.; Meng, J.; Liu, X.; Wu, B.; Han, C.; Mai, L. Comprehensive understanding of the roles of water molecules in aqueous Zn-ion batteries: from electrolytes to electrode materials. *Energy Environ. Sci.* **2021**, *14* (7), 3796−3839.
(145) Pang, Q.; Sun, C.; Yu, Y.; Zhao, K.; Zhang, Z.; Voyles, P. M.; Chen, G.; Wei, Y.; Wang, X. $H_2V_3O_8$ Nanowire/Graphene Electrodes for Aqueous Rechargeable Zinc Ion Batteries with High Rate Capability and Large Capacity. *Adv. Energy Mater.* **2018**, *8* (19), 1800144.
(146) Kasiri, G.; Trócoli, R.; Bani Hashemi, A.; La Mantia, F. An electrochemical investigation of the aging of copper hexacyanoferrate during the operation in zinc-ion batteries. *Electrochim. Acta* **2016**, *222*, 74−83.
(147) Lu, K.; Song, B.; Zhang, Y.; Ma, H.; Zhang, J. Encapsulation of zinc hexacyanoferrate nanocubes with manganese oxide nanosheets for high-performance rechargeable zinc ion batteries. *J. Mater. Chem. A* **2017**, *5* (45), 23628−23633.
(148) Zhang, H.; Liu, Q.; Fang, Y.; Teng, C.; Liu, X.; Fang, P.; Tong, Y.; Lu, X. Boosting Zn-Ion Energy Storage Capability of Hierarchically Porous Carbon by Promoting Chemical Adsorption. *Adv. Mater.* **2019**, *31* (44), 1904948.
(149) Liu, Z.; Cui, T.; Pulletikurthi, G.; Lahiri, A.; Carstens, T.; Olschewski, M.; Endres, F. Dendrite-Free Nanocrystalline Zinc Electrodeposition from an Ionic Liquid Containing Nickel Triflate for Rechargeable Zn-Based Batteries. *Angew. Chem., Int. Ed.* **2016**, *55* (8), 2889−2893.
(150) Suo, L.; Borodin, O.; Gao, T.; Olguin, M.; Ho, J.; Fan, X.; Luo, C.; Wang, C.; Xu, K. Water-in-salt" electrolyte enables high-voltage aqueous lithium-ion chemistries. *Science* **2015**, *350* (6263), 938−943.
(151) Zhang, N.; Cheng, F.; Liu, Y.; Zhao, Q.; Lei, K.; Chen, C.; Liu, X.; Chen, J. Cation-Deficient Spinel ZnMn2O4 Cathode in Zn(CF3SO3)2 Electrolyte for Rechargeable Aqueous Zn-Ion Battery. *J. Am. Chem. Soc.* **2016**, *138* (39), 12894−12901.

https://doi.org/10.1021/acsomega.4c06199
ACS Omega 2024, 9, 47920−47938